https://doi.org/10.5194/egusphere-2026-942
Preprint. Discussion started: 4 March 2026

Net ecosystem exchange of extensive green roofs: the role of coupled energy, carbon, and water fluxes quantified by long-term micrometeorological observations

Niklas Markolf[1], Stephan Weber[1]

[1]Institute of Geoecology, TU Braunschweig, Braunschweig, 38106, Germany

Correspondence to: Niklas Markolf (n.markolf@tu-braunschweig.de)

Abstract. Vegetated roofs (i.e. green roofs, GRs) have been emerging as a promising nature-based solution in urban environments to mitigate climate change impacts, such as heat waves, urban flooding, and increased greenhouse gas emissions. Green roofs were shown to provide various ecosystem services, such as carbon sequestration from the urban atmosphere.

The present study leverages a 9-year time series of continuous, integrated flux measurements on a large, extensive GR in Berlin, Germany, using the eddy-covariance technique. We investigate the coupling between carbon, water, and energy fluxes at different temporal scales to determine their role in shaping the net ecosystem exchange (NEE) of the GR ecosystem.

The extensive GR was a moderate carbon sink with an average annual NEE of -92 g C m^{-2}, ranging from -154 to +8 g C m^{-2} in the study period from 2015–2023. In the final two years, 2022 and 2023, the annual NEE shifted toward net respiration, coinciding with increased nocturnal CO_2 efflux and an abrupt rise in substrate organic carbon, which stemmed from external carbon sources. During the study period, the roof retained 51 % of precipitation, with a strong coupling between soil moisture, evapotranspiration, sensible heat flux, and carbon assimilation. Low substrate water content (below ≈ 0.05 m^3 m^{-3}) reduced evaporative cooling and suppressed carbon assimilation during the summer.

The findings demonstrate the importance of integrated flux monitoring and emphasise the multifaceted environmental benefits of extensive GRs while also pointing to their structural constraints.

https://doi.org/10.5194/egusphere-2026-942
Preprint. Discussion started: 4 March 2026

1 Introduction

Urban environments are increasingly challenged by the combined pressures of climate change and population growth. As the global urban population continues to rise (United Nations, Department of Economic and Social Affairs, Population Division, 2019), expanding settlement areas and impervious surfaces exacerbate flooding risks, elevate greenhouse gas emissions, and modify the surface energy balance, leading to the urban heat island effect (Oke, 1982). To address these challenges, sustainable and multifunctional solutions are required. Nature-based solutions (NBS) have proven effective in mitigating such negative impacts by restoring ecosystem functions within cities (Pereira et al., 2023; Ferreira et al., 2022; Soltanifard and Amani-Beni, 2025). However, the limited availability of open space in densely built environments makes their widespread implementation at ground level challenging.

Green roofs (GRs)—vegetated surfaces installed on rooftops—offer a promising form of NBS that can be integrated into both new and existing buildings. Roof areas account for approximately 20–25 % of total urban surfaces (Akbari and Rose, 2008), representing significant potential for urban greening. On a global scale, it is predicted that the available area for green roofs will increase by around 80% between 2022 and 2060 (Ürge-Vorsatz et al., 2025), underscoring their future relevance as an urban nature-based solution. GRs deliver multiple ecosystem services, including stormwater retention (Stovin et al., 2012; Schultz et al., 2018; VanWoert et al., 2005; Stovin, 2010; Liu et al., 2019), local air temperature regulation through evapotranspiration cooling (Heusinger et al., 2018; Francis and Jensen, 2017), and carbon sequestration (Heusinger and Weber, 2017b; Konopka et al., 2021; Starry et al., 2014; Teemusk et al., 2019). Their performance, however, depends on design and maintenance factors, particularly substrate depth and vegetation type. While intensive GRs support diverse vegetation due to larger substrate depths, extensive GRs, characterised by shallow substrates and drought-resistant plants such as *Sedum*, are lighter, require less maintenance, and can be applied more widely. In Germany, 86 % of newly constructed GRs in 2023 were extensive systems (Mann and Landwehr, 2024) with a similar value of 84 % reported for Austria for 2022 (Formanek et al., 2024).

Research on green roof surface–atmosphere exchange documents the potential of GRs to sequester carbon from the atmosphere via photosynthesis. Konopka et al. (2021) measured the carbon exchange of an extensive GR located in Berlin, Germany (same GR as in the present study) via eddy covariance (EC) over the course of 5 years (September 2014 until August 2019) and found a consistent annual net assimilation of carbon with an average of -141 g C m^{-2}. For the same GR, Hansen et al. (2025) reported a net carbon assimilation of -14 g C m^{-2} over the study period of 24 June to 10 November 2022 as observed by EC, and a net assimilation of -51 g C m^{-2} as observed by soil chambers. Getter et al. (2009) found that an extensive green roof system in Michigan, USA, sequestered -187 g C m^{-2} per year in above- and belowground biomass and substrate organic matter.

Existing studies demonstrated green roofs to be a moderate sink for carbon, however, long-term studies examining the variability of the GR carbon exchange over multiple years are scarce. Additionally, little is known on how the boundary conditions, i.e. temporal dynamics of surface energy balance and water fluxes, play a role in shaping the carbon exchange of GRs.

https://doi.org/10.5194/egusphere-2026-942
Preprint. Discussion started: 4 March 2026

Better insight into these interactions, however, is essential for evaluating GR carbon sequestration potential, resilience, and contribution to urban climate adaptation and mitigation.

The present study introduces a nine-year eddy covariance dataset on carbon, water, and energy fluxes from a large, extensive green roof in Berlin, Germany. We hypothesise that the extensive green roof is a sink for carbon and investigate to what extent water, and energy fluxes jointly shape the net ecosystem exchange and ecosystem service provision. By integrating these components, this study provides a comprehensive empirical assessment of extensive GR functioning, supporting modelling of urban ecosystem services and evidence-based strategies for sustainable city design.

https://doi.org/10.5194/egusphere-2026-942
Preprint. Discussion started: 4 March 2026

2 Material and Methods

2.1 Study site

Data has been collected on an extensive GR in northeast Germany located on a multi-storey car park at Berlin-Brandenburg Airport (BER; lat: 52.37°; lon: 13.51°, Fig. A1). The GR is located southeast of the city centre of Berlin on plain level terrain at a height of 61 m asl. The roof has a slope of about 2 %, a size of 8,600 m^2 and was built in 2012. The substrate composition is mainly expanded shale, expanded clay, lava, pumice and compost with a depth of 9 cm (Table 1). Initial substrate organic matter content, which was determined by loss-on-ignition, was 3.1 %, according to the manufacturer's specification. The roof is non-irrigated and has been initially planted mainly with *Sedum* and *Phedimus* species. Vegetation height varies between 0.1 and 0.3 m throughout the year. Plant surface coverage, as estimated from photographs taken at regular intervals (usually every 1–2 months) from up to 11 fixed spots distributed evenly throughout the GR (Heusinger and Weber, 2017a), increased from about 41 % in the summer of 2015 to ≈ 62 % in 2023 (Fig. A2a). Additional information about the site and substrate properties can be found in Table 1.

Table 1: Location and properties of the studied green roof.

	BER green roof site
Coordinates	lat: 52.37°; lon: 13.51°
Construction finished	May 2012
Size [m^2]	8 600
Slope [%]	2
Plant coverage [%]	≈ 62 (summer 2023)
Dominant plant species	*Sedum album* and *-acre*, *Phedimus spurius* and *-kamtschaticus*
Substrate	Optigrün M-leicht
-composition	lava, pumice, expanded shale, expanded clay, compost
-depth [cm]	9
-maximum volumetric water content [%]	42.3
-porosity [%]	71
- organic matter [%]	3.1
-dry bulk density [g cm^{-3}]	0.78
-bulk density at water saturation [g cm^{-3}]	1.22

2.2 Instrumentation and data processing

The study period lasted for 9 years from 01 January 2015 to 31 December 2023. In 2024, photovoltaic panels were installed across the entire BER roof, which prevents further analysis of the green roof–atmosphere exchange under the same conditions after the end of 2023. Carbon, water and sensible heat fluxes were measured using the eddy covariance technique with a

https://doi.org/10.5194/egusphere-2026-942
Preprint. Discussion started: 4 March 2026

temporal resolution of 10 Hz (Table 2). A Campbell Scientific CSAT3A sonic anemometer and an EC150 open-path infrared gas analyser were installed at a height of 1.15 m above roof level. Meteorological variables included air temperature, relative humidity and all four components of the radiation balance. The volumetric water content (VWC) of the substrate was measured at a substrate depth of 5 cm using Campbell Scientific VWC probes, applying the time-domain reflectometry method. The ground heat flux was measured with a Hukseflux heat flux plate located 5 cm deep in the substrate and corrected for heat storage above the heat flux plate using a soil temperature sensor and the calorimetric method (Liebethal et al., 2005; Weber, 2006). All data were stored with a 30-minute time resolution.

The EC data were post-processed using the Eddy Pro software Version 7.0.9 (Fratini and Mauder, 2014; LI-COR Biosciences, 2022) according to established procedures in the EC community (Aubinet et al., 2012). The data processing workflow is based on procedures as documented in Konopka et al. (2021) but will be briefly summarised in the following: Spectral correction was applied according to Moncrieff et al. (1997), and despiking of the data was performed. Quality flags were calculated according to Foken et al. (2005), and flags ≥ 7 were rejected. Furthermore, data were rejected when CO_2 and H_2O signal strengths were < 0.7 and data during and 30 minutes after precipitation were rejected. Data from the wind sector (36°–54°), which is the sector where the measurement tripod affects data, was also excluded. The final data availability was 66 % for CO_2 and latent heat fluxes and 75 % for sensible heat fluxes. Missing data were gap-filled using the Look-Up-Tables (LUT) and Mean Diurnal Variation (MDV) approaches (Falge et al., 2001a; Falge et al., 2001b; Reichstein et al., 2005). The LUT algorithm uses data from similar meteorological conditions to replace missing values. If similar meteorological conditions are not found, the MDV approach is used, which is based on temporal-autocorrelation of the fluxes. We follow the standard micrometeorological sign convention: a negative flux is a flux directed towards the surface, whereas a positive flux is a flux directed away from the surface. Furthermore, daytime is defined for gap-filled data with a global radiation value of > 10 W m^{-2}.

Table 2: Overview of measurement setup at BER. Abbreviations: u,v,w = wind vectors, T_S = sonic temperature, S = shortwave radiation, L = longwave radiation, ↓ = downward, ↑ = upward, VWC = volumetric water content.

Quantity	Device	Measurement height above (+) / below (-) roof level [m]	Sampling frequency
u, v, w, T_S	CSAT3A	1.15	10 Hz
CO_2, H_2O mass densities	EC 150	1.15	10 Hz
S↑, S↓, L↑, L↓	Huskeflux NR01	2	5 s
Air temperature and air humidity	Vaisala HMP155	2	5 s
Soil temperature	CS 107	-0.025	5 s
VWC	CS TDR probe	-0.05	5 s
Substrate heat flux	Hukseflux HFP01SC	-0.05	5 s

https://doi.org/10.5194/egusphere-2026-942
Preprint. Discussion started: 4 March 2026

2.3 Data quality control

Heusinger and Weber (2017a) documented that the conditions found at BER, e.g. turbulence development, complied with the principles of EC. Measurement setup was the same during the 9-year study period; nonetheless, the data quality and turbulence development were checked for the present data set to investigate potential differences over time. As indicators, turbulence spectra as well as integral turbulence characteristics were calculated.

The integral turbulence characteristic, given by the ratio of the standard deviation of the vertical wind velocity (σ_w) to friction velocity (u*) under neutral stratification, was calculated for different wind directions to assess turbulence development above the GR. The influence of roughness elements on EC measurements was analysed using the aerodynamic roughness length (z_0), calculated from the logarithmic wind profile.

Cospectra were calculated for each flux-averaging period using Eddy Pro. The program outputs "binned" cospectra by dividing the frequency range into 50 exponentially spaced frequency bins and averaging individual cospectral values that fall within each bin. This reduces noise that typically affects medium and high-frequency ranges. Subsequently, the program calculates ensemble-averaged cospectra for the whole study period that are quality controlled and sorted according to the atmospheric stability regime, defined by the value of the Obukhov length (L; unstable: -650 m < L < 0 m; stable: 0 m < L < 1000 m).

To check for potential contributions to the measured flux from areas outside the GR, we calculated the aggregated flux source area (FSA) using the FFP model (Kljun et al., 2015). The input parameter of the boundary layer height (h) was assumed as a fixed value of 1500 m. Kljun et al. (2015) reported minor influence on FSA dimensions when changing the value of h by ±20 % (up to ±3.7 % change in FSA peak location under stable conditions), indicating a low model sensitivity for h.

2.4 Analysis of substrate carbon content

Multiple bulk substrate samples for laboratory carbon content analysis were taken every May or June at randomly selected locations on the GR starting in 2020. In the laboratory, the plant material (roots, leaves, etc.) was first removed from the substrate samples. A mortar and pestle were used for crushing, grinding, and mixing each sample. Subsequently, total carbon (C), nitrogen (N) and sulfur (S) in all solid samples were measured by means of an elemental analyser (EuroEA 3000, HEKAtech GmbH, Germany) that combusted 10–20 mg aliquots of each sample in a tin capsule calibrated with a sulfanilamide standard (CD41:750:17 %; ND16:260:22 %; SD18:640:18 %) and BBOT (2.5-Bis(5-tert-butyl-benzoxazol-2-yl)thiophene; CD72.52 %; ND6.51 %; SD7.44 %). The quality of the measurements was controlled by three certified reference materials - NIST 1515 apple leaves (ND2:250:19 %), NCG DC 73030 Chinese soil (CD0:6170:044 %; SD0:20:03 %), MOC soil standard (CD3:190:07 %; ND0:270:02 %; SD0:0430:005 %) - and sulfanilamide (1 for every 10 analyses).

Samples were not acidified prior to elemental analysis, so the measurements represent total carbon (TC). However, because the substrate consists exclusively of non-carbonate mineral aggregates and contains no carbonate-bearing components, inorganic carbon was assumed to be negligible, and the TC values will therefore be interpreted as total organic carbon (TC ≈ TOC).

In contrast to the laboratory measurements, the manufacturer's value of 3.1 % represents organic matter determined by loss-on-ignition, a method that quantifies total mass loss upon combustion and therefore includes true organic material as well as

https://doi.org/10.5194/egusphere-2026-942
Preprint. Discussion started: 4 March 2026

volatilised structural water and thermally unstable mineral fractions. Hence, the two metrics cannot be directly compared. However, the initial TOC range of 1.5–2.5 % was considered plausible based on the substrate composition (Table 1).

A mass-balance comparison between substrate TOC and measured EC carbon fluxes was conducted (Sect. 3.4.3, Fig. 11) with the following procedure: Substrate TOC for both the measured values (2020–2023) and the initial value (2012) were converted to g C m^{-2}. The values for the other years (2013–2019) have been linearly interpolated. In order to analyse the potential range of substrate TOC, two assumptions were made: 1) the initial TOC was set at 1.5 %, and bulk density was fixed at 0.78 g cm^{-3} (lower bound), and 2) the initial TOC was set at 2.5%, and bulk density increased to 1.18 g cm^{-3} in 2020 (upper bound). For the mass-balance comparison, we added the annual carbon sequestration (2015–2023) from EC flux observations to the initial TOC value. For the years 2012–2014, where flux measurements were not yet operational, we assumed a value of 121 g C m^{-2} a^{-1}, i.e. the average for the period 2015–2021.

2.5 Water balance

The water balance is written as:

$$P = Q + ET + \Delta S \quad (1)$$

with P = Precipitation, Q = Runoff, ET = Evapotranspiration and ΔS = Change in storage.

It is a common practice to neglect changes in the water storage (ΔS) over annual/multi-annual periods in natural ecosystems, because it is minor when compared to the fluxes of the other components (Xue et al., 2013; Greve et al., 2016). Some studies, however, found that ΔS cannot be neglected in the annual water balance (Han et al., 2020; Bruno et al., 2022). The water storage capacity of the BER green roof was found to be 35.8 mm, i.e. maximum possible ΔS (Markolf et al., 2024), indicating its minor contribution to the water balance. The water storage experiences fast fluctuations of storage levels due to the shallow substrate, indicating that water has a short residence time before it leaves the GR via evapotranspiration (ET) or runoff, i.e. extensive GRs are not comparable to natural ecosystems with groundwater access. Hence, we decided to neglect ΔS in the annual water balance. Due to the fact that P and ET are measured variables in this study, we attribute the residual to Q (Q = P - ET). Not measuring Q, but calculating it as a residual of the water balance, raises uncertainties in this term. However, by calculating the ratio of ET to P for annual and multi-annual periods, we are able to retrieve an indicator of the volumetric water retention by the GR.

2.6 Statistical analysis

To evaluate whether there is a statistically significant monotonic trend of a parameter over the study period, two non-parametric rank-based tests were applied. Spearman's rank correlation assesses the strength and direction of a monotonic relationship between a variable and time by converting the data values to ranks and calculating a correlation coefficient (ρ) between the ranked data and the ranked time sequence. In addition, the Mann-Kendall trend test was used, which evaluates all pairwise comparisons among data points and determines whether later values tend to be systematically larger or smaller, expressed by the Kendall's τ statistic. The p-value determines whether the observed trends are unlikely to have occurred by chance, and

https://doi.org/10.5194/egusphere-2026-942
Preprint. Discussion started: 4 March 2026

statistical significance was evaluated at a threshold of $p = 0.05$. Both methods are robust to non-normality and outliers (Croux and Dehon, 2010), making them suitable for time-series data with limited sample sizes.

https://doi.org/10.5194/egusphere-2026-942
Preprint. Discussion started: 4 March 2026

3 Results

3.1 Meteorological conditions during the study period

Dominating wind directions at BER are from the sectors W to SSW and E to ENE (Fig. 1). Wind directions 36°–54° were excluded in the quality control process (cf. Sect. 2.2). Wind speed is 2.75 ± 1.5 m/s on average, but peaks in wind speed are distinctly higher (maximum of 30.3 m s^{-1}) due to the exposed location in the North German plain. Mean air temperature was 11.1 °C over the study period, and mean annual precipitation sum was 494 mm (Fig. 2b). Mean air temperature was highest in 2019 (11.6 °C), and lowest in 2021 (10.3 °C), and precipitation was highest in 2023 (736 mm), 2.5 times as much as in the driest year, 2018 (295 mm).

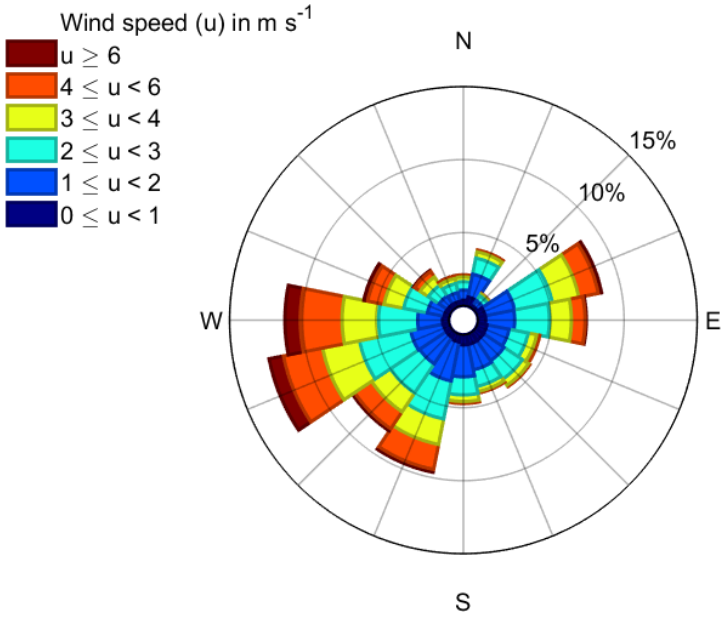

Figure 1: Wind rose showing the frequency of individual wind directions and wind speeds at BER during the study period.

Precipitation was evenly distributed over the year, i.e. no rainy seasons (Fig. 2a), but more dry days occurred in summer due to convective rainfall, i.e. less frequent, but heavier events. Air temperature showed clear seasonality: highest temperatures were reached during the summer months (June, July, August), where daily maxima of ≥25 °C occurred (53 days per year on average). The coldest months are December, January and February, where temperatures often fell below the freezing point (56 days per year on average). Temperatures ranged between -13.4 °C and 37.9 °C during the study period.

https://doi.org/10.5194/egusphere-2026-942
Preprint. Discussion started: 4 March 2026

Compared to data from the 30 years reference period (1991–2020) at the German Weather Service (DWD) station located near the GR (BER: Berlin Brandenburg, DWD-ID 427, 46 m asl., distance 1.9 km) all the years during the study period were warmer than the average (Fig. 2b), with 4 years (2015–2017,2021) showing lower deviations from the reference period (≤ +0.7 °C) and 5 years showing higher deviations (≥ +1.4 °C). Only 2017 and 2023 had higher precipitation sums than the average of the reference period (117 % and 141 %, respectively), but many years were close (86–99 %). The year 2022 and especially 2018 experienced precipitation sums well below the average of the reference period (77 % and 57 %, respectively). Yearly ET varies between 194 mm in 2018 and 315 mm in 2017 (Fig. 2c). The ratio of yearly ET to yearly precipitation, which is indicative of retention (cf. Sect. 2.5), is between 0.49 and 0.58, except for the drought year 2018 (0.66) and the wettest year 2023 (0.38). Considering the whole study period, the ratio was 0.51.

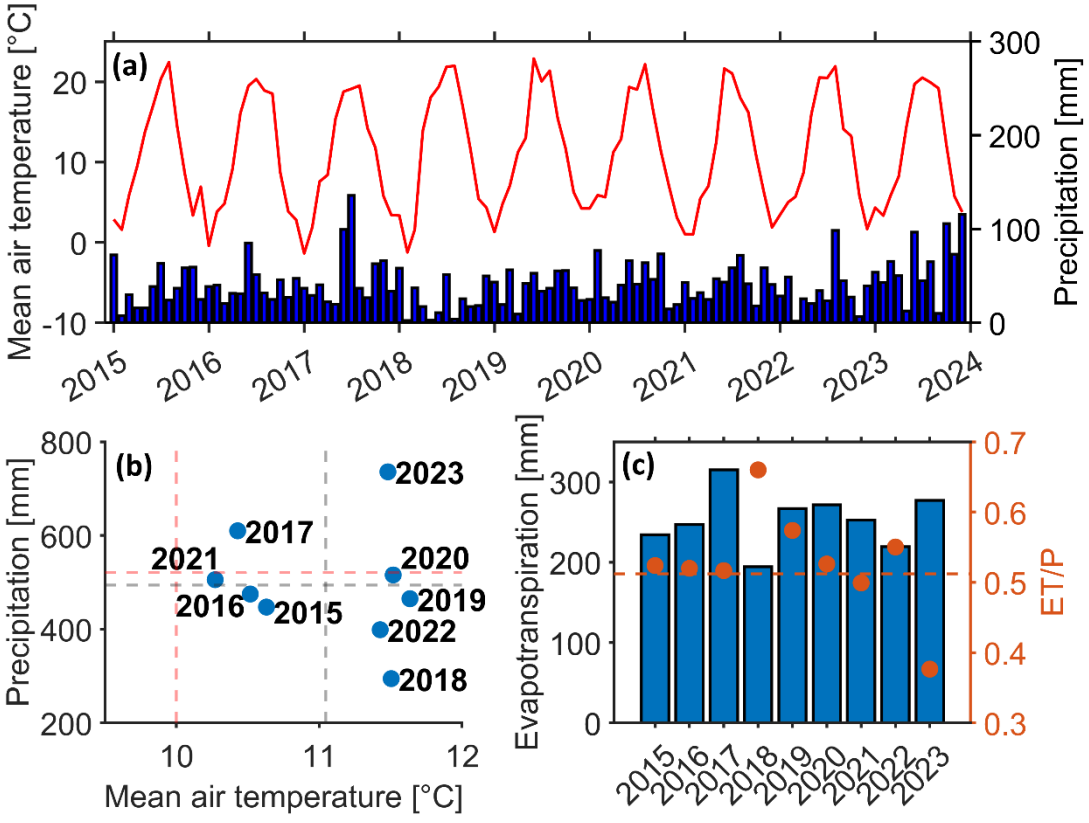

Figure 2: (a) Monthly mean air temperature and precipitation sum for the whole study period. (b) Mean air temperature and precipitation sum for every year of the study period. Grey, dashed lines indicate the mean from the study period and red, dashed lines indicate the mean from the reference period (1991-2020, from DWD station 427). (c) Annual evapotranspiration (ET) sums and ratio of ET sum to precipitation sum (P) for every year (circles) and the whole study period (dashed, horizontal line).

https://doi.org/10.5194/egusphere-2026-942
Preprint. Discussion started: 4 March 2026

3.2 Data quality

The integral turbulence characteristic under neutral stratification is $\sigma_W/u^* = 1.33$ on average with low variation across wind directions (Fig. A3a). This is very close to the value of 1.25 as proposed for well-developed homogeneous turbulence under neutral stratification (Foken and Mauder, 2024). Aerodynamic roughness length (z_0) is consistent throughout wind directions (Fig. A3b), indicating homogeneous vegetation heights across the GR and minor influence of roughness elements on EC measurements (mean = 0.04 m).

The normalised cospectra for unstable stratification (-650 m < L < 0 m; Fig. A4) exhibit the expected turbulent structure with clear peaks at the expected normalised frequencies, consistent scalar behaviour, and an inertial-subrange decay close to the theoretical $f^{-4/3}$ slope. CO_2 and H_2O cospectra show an enhanced contribution to gas flux from lower frequencies, i.e. larger eddies, and typical high-frequency dampening when compared to the w'T' cospectrum. The cospectra indicate that the data exhibit good quality, as the expected patterns of turbulence and flux are present with minimal noise or distortion.

The 80 % FSA extends at a maximum of 39 m and 36 m towards the dominating wind direction and over an area of 2550 m^2 and 1860 m^2 for night- and daytime respectively (Fig. 3). The peak contribution is situated in the sector 200 ° to 300 °at a distance of approx. 2.5 m to the EC station. The 70 % FSA is located entirely within the GR, whereas the 80 % FSA extends beyond the GR, but only at the northern edge (277°–13°), where fetch is the smallest. The nocturnal 80 % FSA exceeds the GR by a maximum of 4.8 m. The area exceeding the GR accounts for 4.7 % of the total area; however, it contributes < 1 % to the total flux since wind from North is rare at BER (Fig. 1).

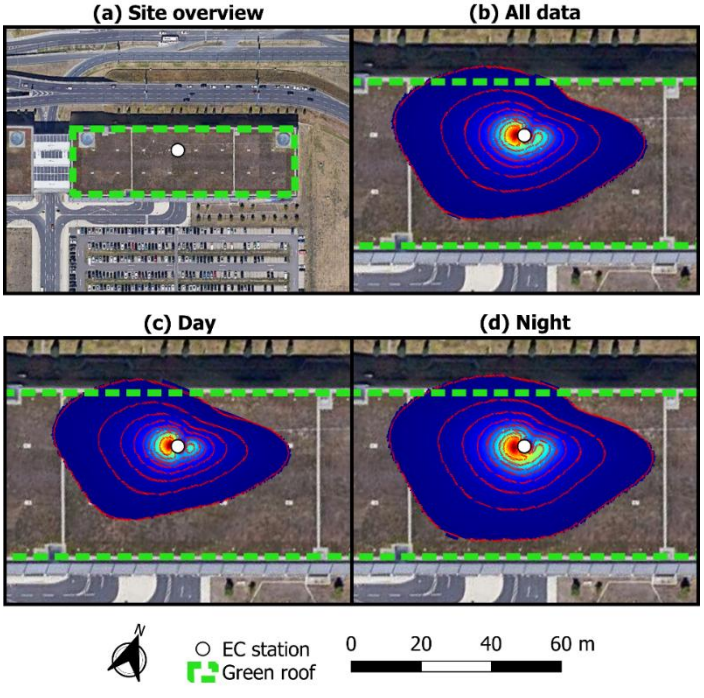

Figure 3: (a) Site overview. Flux source area calculated by the FFP model (Kljun et al., 2015), aggregated for the whole study period (b), daytime (c) and night-time (d). The scale refers to (b), (c) and (d) only. Basemap: © Google Satellite.

https://doi.org/10.5194/egusphere-2026-942
Preprint. Discussion started: 4 March 2026

3.3 Surface energy balance and water exchange

Peak flux density is reached around noon for the shortwave components of the radiation balance and in the early afternoon for the longwave components, corresponding to the time when substrate and atmosphere temperatures reach their daily maxima (Fig. 4a). The ratio of reflected to incoming shortwave radiation (albedo) is 19 % for the study period (Table 3). Available energy for turbulent heat fluxes is obtained as net radiation (Q*) minus ground heat flux (Q_G). Energy balance closure, derived from the regression between available energy and turbulent heat, is 79 %, indicating a 21 % closure gap (Fig. A5).

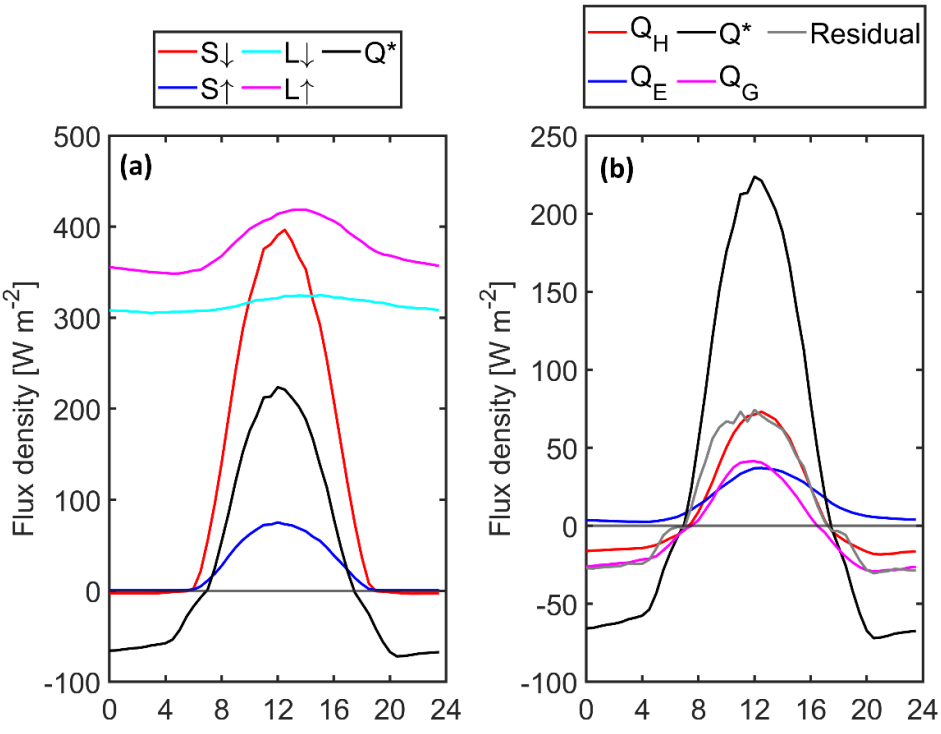

Figure 4: Median diurnal cycle of (a) radiation balance and (b) energy balance components for the entire study period. S = shortwave radiation, L = longwave radiation, ↓ = downward, ↑ = upward

In the median diurnal cycle of the energy balance components, sensible heat flux (Q_H) is negative during night-time (Fig. 4b), indicating that heat is transported from the warmer atmosphere towards the colder GR surface. Also, heat is transported in the substrate towards the cooler surface. During daytime, the flux changes direction, and Q_H and Q_G become positive, warming the air above the GR and heat is transported into the substrate. Latent heat flux (Q_E) is positive throughout the diurnal cycle. However, there are individual events during the study period where Q_E becomes negative during night and water vapour is transported towards the surface, i.e. dew formation. Q_H is larger than Q_G and Q_E during the day, and the fluxes peak at noon, when the residual (i.e., the difference between Q* and the sum of the three other components) is largest.

https://doi.org/10.5194/egusphere-2026-942
Preprint. Discussion started: 4 March 2026

The Bowen ratio (β), representing the ratio of sensible to latent heat fluxes, is a diagnostic metric that characterises the distribution of available energy between turbulent heat transfer to the atmosphere and the energy consumed by phase change through evapotranspiration. During winter (DJF) and during the night, β often becomes negative (Table 3) due to a negative Q_H, when heat is transported from the warmer atmosphere towards the cooler GR. During spring (MAM) and summer (JJA), there is more energy available, leading to larger substrate heat storage and stronger positive fluxes. During the day, β is at least 1 during all seasons except for winter and is highest during the summer months. Considering all data, β is > 1 for spring and summer and 0.25 during autumn (SON). For the whole 9-year study period, β was close to 1.

Table 3: Bowen-ratio (β) for the seasons, the whole study period (SP) and day- and night-time. The median (daytime) albedo as well as the mean evapotranspiration (ET) sum is given for the individual seasons and the whole study period. DJF = winter, MAM = spring, JJA = summer, SON = autumn.

	DJF	MAM	JJA	SON	SP
β	-1.09	1.23	1.70	0.25	0.94
β (day)	0.05	1.81	2.05	1.08	1.62
β (night)	-2.75	-2.99	-2.64	-4.76	-3.15
Albedo [%]	17	19	19	19	19
ET [mm]	31	74	101	47	2278

There is a strong dependence of β on VWC (Fig. 5a), i.e. water availability for ET. If water availability is not limited, energy is primarily partitioned into latent heat flux ($\beta < 1$), resulting in reduced sensible heat exchange and a lower ambient temperature (Fig. 5b). This effect diminishes once moisture levels are below VWC ≈ 0.05 m^3 m^{-3}. At that threshold, β increases strongly, and energy partitioning into Q_H is larger, thus reducing the cooling effect of the GR.

https://doi.org/10.5194/egusphere-2026-942
Preprint. Discussion started: 4 March 2026

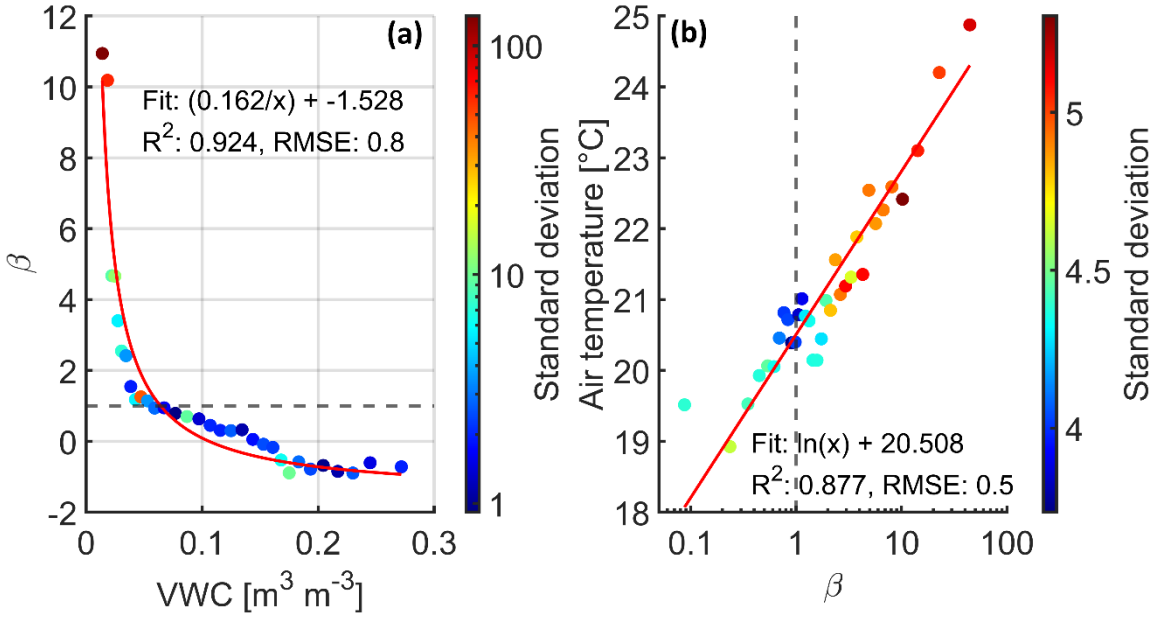

Figure 5: (a) Dependence of the Bowen-ratio (β) on volumetric water content (VWC). Daily averages of VWC were sorted according to their value. A new bin was created every 100 values, and for each bin, the median β was calculated and assigned to the mid-value of the bin. A hyperbolic fit was calculated. β =1 is indicated by the dashed, horizontal line. (b) Dependence of the air temperature on β. Half-hour values, restricted to the summer and daytime, were sorted according to their value. A new bin was created every 600 values.

https://doi.org/10.5194/egusphere-2026-942
Preprint. Discussion started: 4 March 2026

3.4 Carbon exchange

3.4.1 Median diurnal cycles of the carbon flux

During night-time the carbon exchange between the GR and atmosphere showed net positive fluxes, representing net respiration (Fig. 6). The magnitude of nocturnal respiration ranged between +0.85 µmol m^{-2} s^{-1} and +1.63 µmol m^{-2} s^{-1} and was larger during the first hours of the night (compared to the last) and larger during the last 4 years of the study period (2020–2023) than during the first period (2015–2019). During daytime, the median diurnal cycle showed net negative fluxes, i.e. net assimilation of carbon due to photosynthesis. Peak magnitude was reached around noon and ranged between -3.61 µmol m^{-2} s^{-1} (2020) and -1.81 µmol m^{-2} s^{-1} (2023). Hence, the range of annual daytime variation of carbon fluxes is considerably larger than the nocturnal variation.

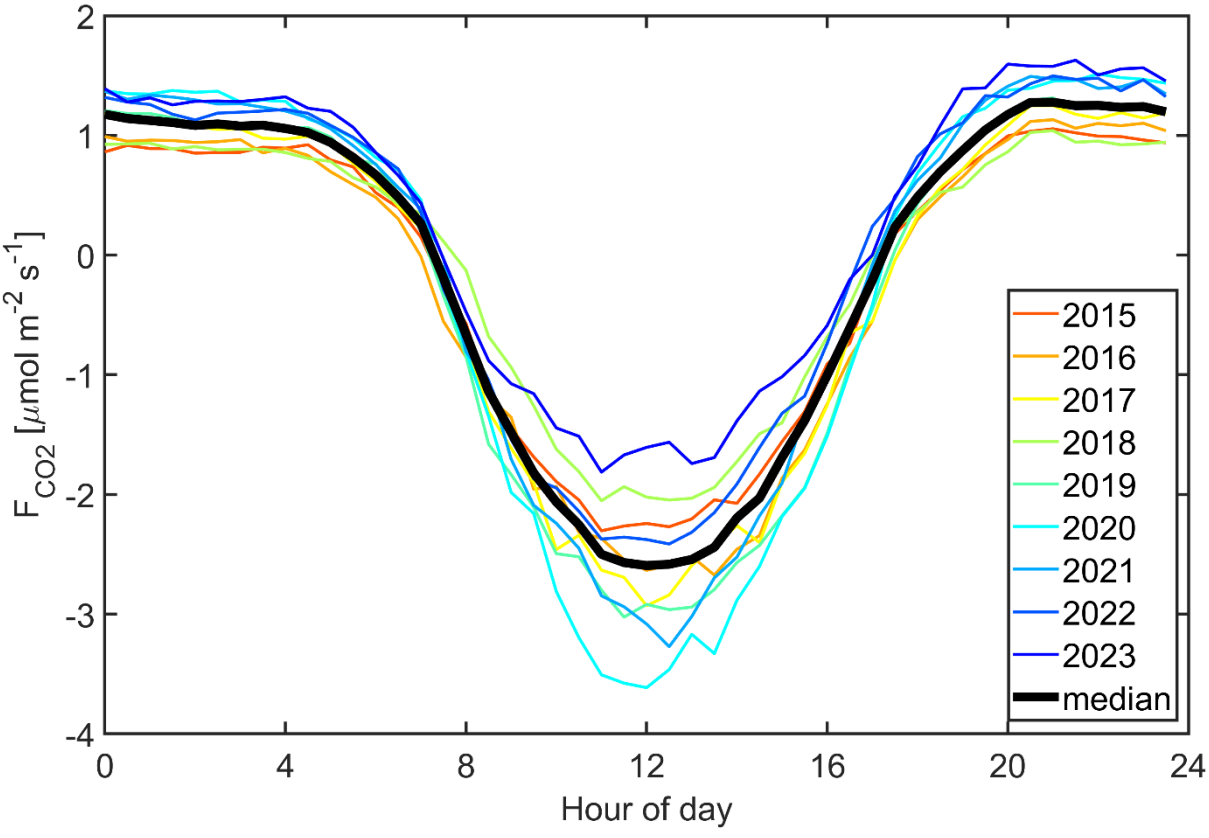

Figure 6: Median diurnal cycle of the carbon flux over the whole study period and for each year.

Towards summer, the magnitude of the fluxes increased (Fig. 7), especially during daytime, but also at night (i.e. higher respiration). Highest daytime net assimilation rates were observed during April and May, and lowest during December and January. The highest nocturnal net respiration rates were observed during June and July, and the lowest during winter. Length of the net assimilation and net respiration phases during the day varies according to the timing of sunrise and sunset and

https://doi.org/10.5194/egusphere-2026-942
Preprint. Discussion started: 4 March 2026

ambient weather conditions. The standard deviation shows that for each month, the flux can vary significantly at a certain time of the day. The standard deviation is largest between 9–12 h and during summer, and lowest during the night and winter.

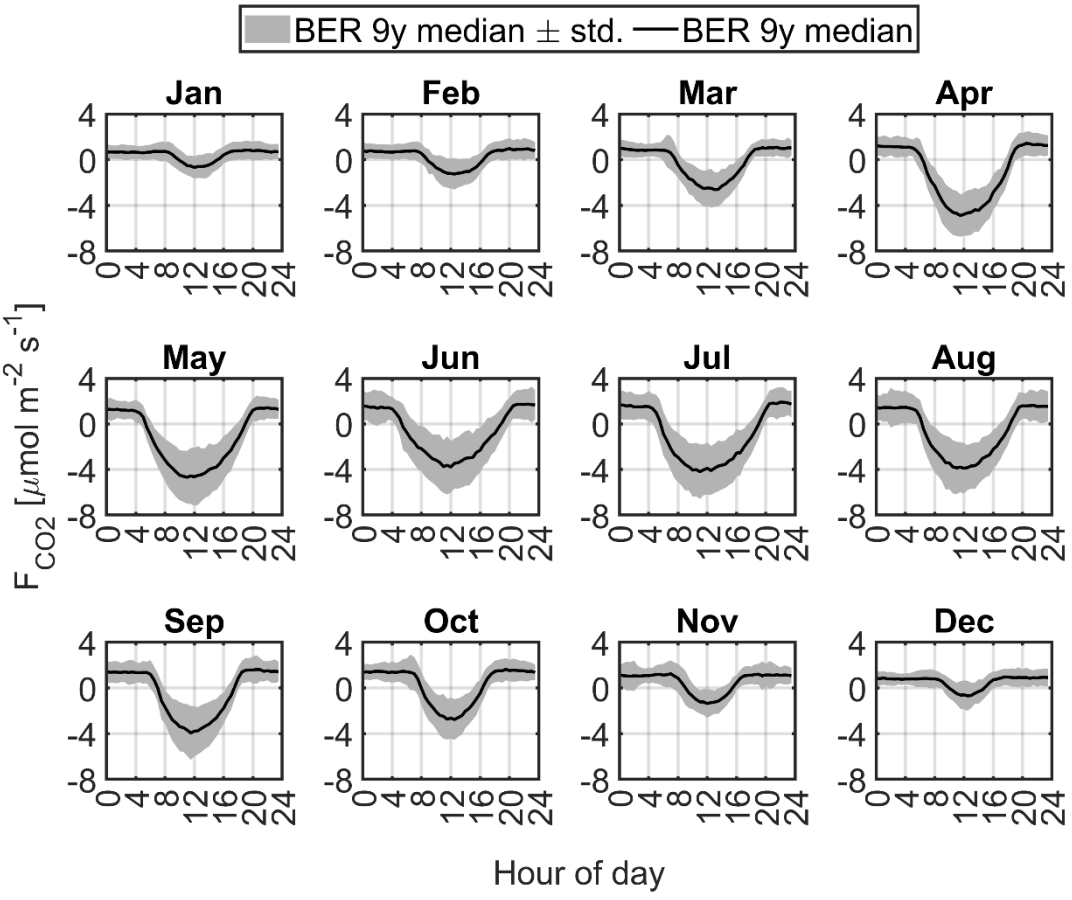

Figure 7: Median diurnal cycle of the carbon flux, separately for January to December, with standard deviation (grey).

260

https://doi.org/10.5194/egusphere-2026-942
Preprint. Discussion started: 4 March 2026

3.4.2 Net ecosystem exchange

The BER green roof was a carbon sink, i.e. net carbon assimilation, in the first 7 study years (Fig. 8), ranging from -154 g C m^{-2} (2017) to -75 g C m^{-2} (2018). In 2022 and 2023, however, the roof proved to be a slight source of C. On average, the site annually sequestered -92 g C m^{-2} in the period from 2015–2023. The cumulative sum of carbon flux displays a clear seasonality, increasing from the start of the year until February or March (or until April in 2023; representing the source season), then decreasing during the vegetation period until September or October (the sink season), after which it begins to rise again. During the sink season, phases of net respiration occur during several years (i.e. 2021). Such intermittent net respiration phases last up to 2 weeks and are often induced by rewetting of the substrate, following dry phases. The Birch effect (Birch, 1958) describes that soil drying and rewetting causes a burst of microbial activity and rapid decomposition (Stage 1) followed by a slower rate (Stage 2), leading to significant carbon release. During spring and summer, there is a net assimilation of carbon, while during winter and usually also during fall, a net respiration of carbon is observed (Fig. 9). On average, the highest net assimilation occurs during May, and the highest net respiration during December. The magnitude of net assimilation during summer shows a positive linear relationship with the plant coverage for the years 2015–2020, which diminished after 2020 (Fig. A2b).

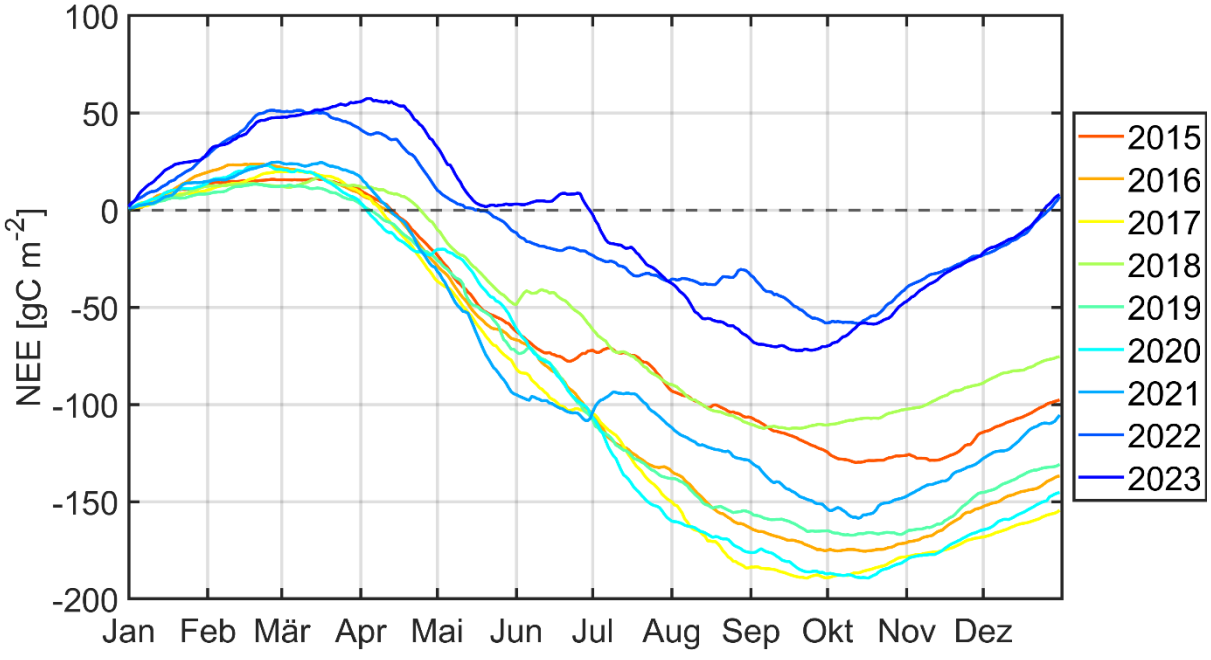

Figure 8: Cumulative sum of the carbon flux (NEE) for every year of the study period.

https://doi.org/10.5194/egusphere-2026-942
Preprint. Discussion started: 4 March 2026

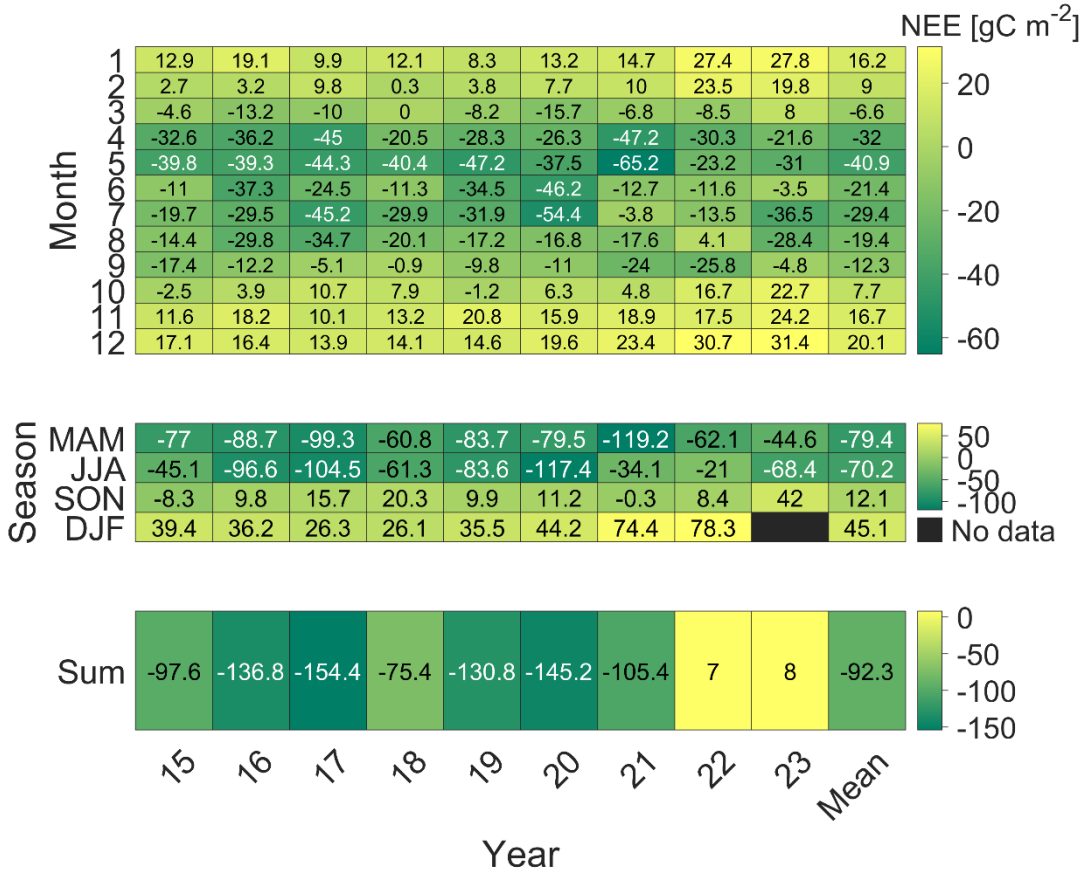

Figure 9: Heatmap containing the cumulative net ecosystem exchange (NEE) for every month, season and year of the study period. DJF = winter, MAM = spring, JJA = summer, SON = autumn.

275 The timings of the sink season are similar between all study years except for 2023, where the sink season is short (Fig. 10). For the sink seasons, the net assimilation rate and the NEE do not show a significant trend over the years of the study period (Table A1). For the source seasons, NEE shows a significant increase, while an increase in the net respiration rate is only significant at a threshold of $p > 0.1$ for the Spearman test.

https://doi.org/10.5194/egusphere-2026-942
Preprint. Discussion started: 4 March 2026

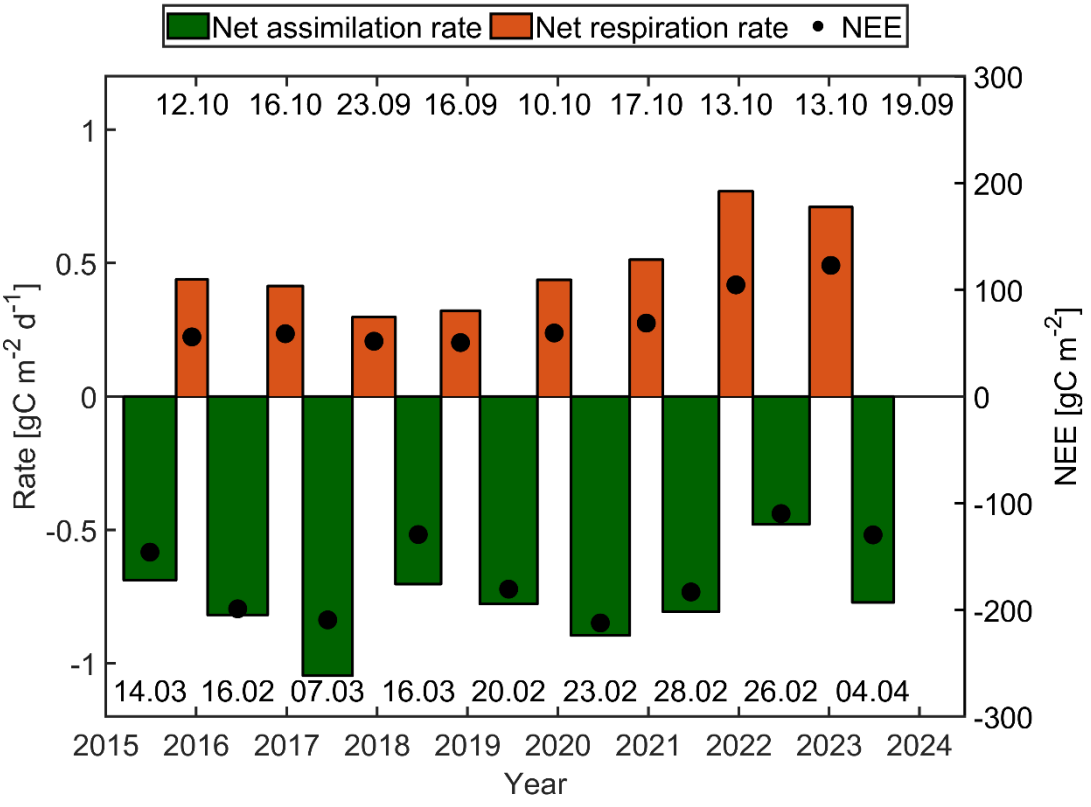

Figure 10: Net sink and net source seasons during the study period. The net assimilation/respiration rate is indicated by the bars, the sum of carbon flux (NEE) by the black circles. The day and month of the beginning of each phase are shown.

https://doi.org/10.5194/egusphere-2026-942
Preprint. Discussion started: 4 March 2026

3.4.3 Influence of environmental parameters on carbon exchange

The previous section has shown (Fig. 8, Fig. 9) that for the last two years of the study period (2022, 2023), the GR has been a net source of carbon, whereas it has been a sink in the prior 7 years. This change of the annual NEE was predominantly driven by increased respiration rather than changes in assimilation (Fig. 6, Fig. 10). Hence, we examined substrate TOC measurements, which were sampled at the site from 2020 to 2023 (cf. Sect. 2.4), for possible changes between the years 2021 and 2022. We found an abrupt increase in substrate TOC from 2021 to 2022 (Fig. 11a), which coincides with the observed changes in carbon flux measured via EC.

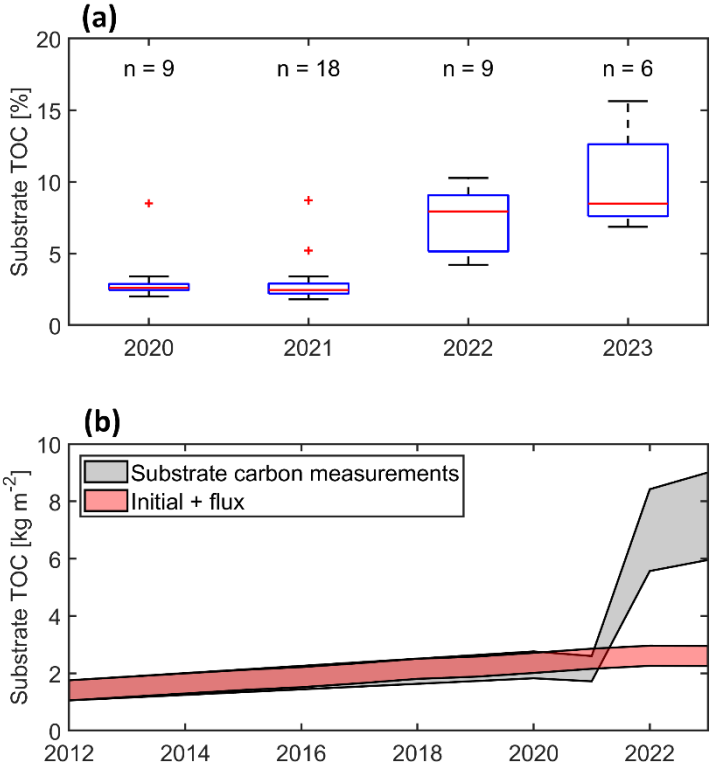

Figure 11: (a) Boxplot showing the substrate total organic carbon (TOC) at BER for individual years (2020-2023) together with the number of samples (n) collected during that year. The boxplots show the median (red line) as well as the interquartile range (box) and the range within which values are not considered outliers (vertical dashed lines). Outliers are depicted by a red "+". (b) Development of the substrate TOC since the beginning of operation of the green roof in 2012 (grey area). The red area represents the initial TOC value plus the annual carbon sequestration of every year (2015–2023) from flux observations.

We used the initial substrate TOC and added the annually observed NEE value (red area in Fig. 11b). Additionally, we display the substrate TOC that we measured from the substrate samples, and linearly interpolated values between 2012 and 2020. The resulting grey area shows the increase in substrate TOC with different assumptions for changes in the dry bulk density (0.78–1.18 g cm^{-3}) and initial TOC (1.5–2.5 %, cf. section 2.4). It is evident that the increase in substrate TOC is not entirely due to

https://doi.org/10.5194/egusphere-2026-942
Preprint. Discussion started: 4 March 2026

atmospheric carbon sequestration but due to an additional source of carbon, as indicated by the two estimates separating after 2021 (red and grey lines in Fig. 11b).

Carbon flux is also influenced by the environmental conditions on the GR. During winter, higher temperatures lead to increased respiration fluxes due to enhanced activity of soil microbes (Fig. 12a). During autumn, fluxes become positive when the daily mean temperature is < 10 °C and in spring, net assimilation is evident even at colder temperatures. Differences in light availability between the seasons lead to higher net assimilation rates during spring compared to autumn and winter at the same temperature range. In summer, the temperature optimum, at which the highest net carbon assimilation is observed, is between 15 °C and 20 °C daily mean temperature. At temperatures higher than this range, net assimilation is reduced.

Substrate water availability influences carbon flux (Fig. 12b). During spring and summer, droughts (i.e. VWC below ≈ 0.05 m^3 m^{-3}), lead to a reduction in net carbon assimilation by the GR. Higher values result in lower net assimilation during spring. For autumn and winter, this is valid for the whole range of VWC values, due to increased microbial activity in the substrate at higher substrate water contents. The carbon flux has a negative correlation with shortwave-downward radiation (S↓). When the mean daytime S↓ reaches values ≥ 200 W m^{-2} during winter and autumn, net assimilation of carbon is evident (Fig. 12d). Carbon uptake in spring and summer is more negative at the same S↓ values. Highest net carbon assimilation is observed when β is between 1 and 3 during spring and summer.

https://doi.org/10.5194/egusphere-2026-942
Preprint. Discussion started: 4 March 2026

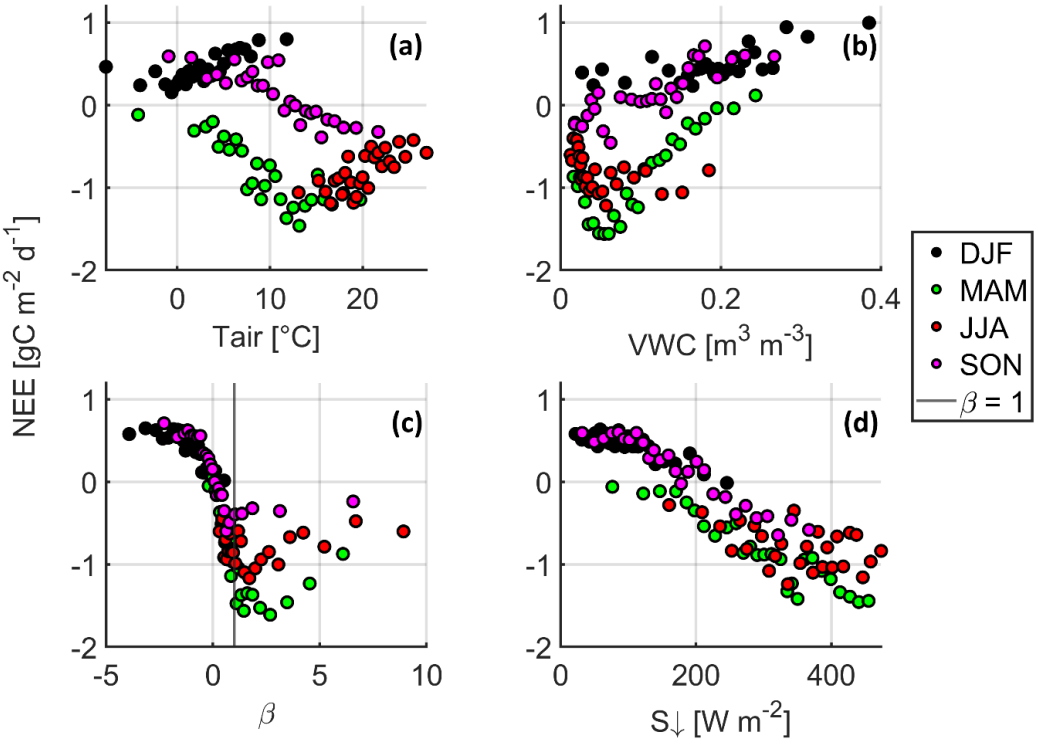

Figure 12: Net Ecosystem Exchange (NEE) in dependence on air temperature (Tair, a), volumetric water content (VWC, b), Bowen-ratio (β, c) and daytime shortwave-downward radiation (S↓,d). Daily means of the independent variables were used and sorted according to their value. A new bin was created every 30 values, and for each bin, the median value of the dependent variable was calculated and assigned to the mid-value of the bin. DJF = winter, MAM = spring, JJA = summer, SON = autumn.

https://doi.org/10.5194/egusphere-2026-942
Preprint. Discussion started: 4 March 2026

4 Discussion

4.1 Net ecosystem exchange and carbon flux dynamics

The annual NEE of the Berlin green roof based on direct turbulent flux measurements using eddy-covariance ranged between -154 g C m^{-2} and 8 g C m^{-2} with an average of -92 ± 62 g C m^{-2} for the period 2015–2023. For the same GR and measurement setup as in the present study, Konopka et al. (2021) documented a consistent annual net assimilation of carbon with an average of -141 g C m^{-2} over the course of 5 years (September 2014 until August 2019). The lower average annual NEE in the present study stems from the slight carbon release during the last two years after consistent annual net uptake in the first 7 years of the study period. Kuronuma and Watanabe (2017) measured the plant and substrate carbon concentrations for *Sedum mexicanum* on a green roof in Chiba (Japan) over a one-year period. They reported annual carbon sequestration values of -276 g C m^{-2} under non-irrigated conditions and -336 g C m^{-2} under regular irrigation. Yang et al. (2023) measured the carbon exchange of an intensive green roof in Nanjing (China) over 1 year using eddy covariance and found the annual NEE to be -17 g C m^{-2}. Getter et al. (2009) found that an extensive green roof system sequestered 375 g C m^{-2} in above- and belowground biomass and substrate organic matter over two years. This results in an average of -187 g C m^{-2} per year. Hence, our result lies at the lower end of the range reported for carbon sequestration in other green roof studies that employed different measurement approaches.

In comparison with natural ecosystems, the green roof shows a lower magnitude of annual NEE, given the structural constraints of extensive systems such as shallow substrates, limited rooting volume, and low water and nutrient availability, restricting vegetation development. Klosterhalfen et al. (2023) , for instance, found the annual NEE of an unmanaged mixed beech forest in central Germany to range between -393 and -670 g C m^{-2} over the period from 2000 to 2022. They reported a decline of carbon uptake by up to 54 % during the drought years 2018, 2019 and 2022. The annual NEE of 19 grassland sites throughout Europe was found to vary between -653 and +171 g C m^{-2}, with an average of -150 g C m^{-2} (Gilmanov et al., 2007). This indicates that natural ecosystems may exhibit large drought-induced variation in carbon uptake, whereas the GR's NEE fluctuates within a relatively narrow range, reflecting the stress tolerance and drought-adapted physiology of its vegetation. Additionally, the GR enables the sequestration of carbon in areas that would otherwise have no capacity for this, effectively converting impervious urban surfaces into carbon sinks.

The carbon flux measurements provide valuable insights into the temporal dynamics of the GR's carbon exchange. The GR shows seasonality in the carbon flux, with the length of the daily net assimilation phase associated with sunrise and sunset timings. Peak net assimilation is reached, on average, during May, followed by April, July, June and August. This suggests that during late spring, conditions are optimal for carbon assimilation due to high light availability accompanied by less extreme temperatures and higher water availability compared to the summer months. Higher incoming radiation and thus energy availability led to increased net assimilation rates, while mean daily temperatures exceeding values of ≈ 20 °C during summer decreased net carbon assimilation, potentially due to stomatal closure to reduce transpiration (Grossiord et al., 2020; McAdam and Brodribb, 2015). There is a clear trend towards lower carbon assimilation by the GR when water availability drops below ≈ 0.05 m^3 m^{-3} during spring and summer. At higher VWC values, there was no effect on carbon fluxes observed during summer,

https://doi.org/10.5194/egusphere-2026-942
Preprint. Discussion started: 4 March 2026

but reduced net assimilation during spring, which might be due to the spring season incorporating colder phases (e.g. March) where VWC is usually high and light availability and thus photosynthesis is low.

These results illustrate how carbon flux is affected by various environmental and biotic factors. During the first five summers, higher plant coverage corresponded to increased net carbon assimilation. In subsequent years, net assimilation was lower at comparable coverage, suggesting that other factors have exerted a stronger influence on carbon fluxes.

The carbon exchange of the GR–atmosphere system was strongly shaped by diurnal patterns, with nocturnal respiration intensifying in the later years of the study (cf. Fig. 6). Correspondingly, annual NEE became slightly positive in 2022 and 2023, after 7 years of consistent net uptake. Our findings indicate that higher respiration, rather than changes in assimilation, caused the observed change in annual NEE. While sink season NEE showed no long-term trend, source season NEE increased significantly. During the last two source seasons, temperatures did not exceed those of previous years, but they showed the highest mean VWC value. Studies show that microbial activity and soil respiration increase with soil temperature and peak at moderate levels of VWC, where they are not constrained by low water availability or by oxygen limitation under excessive soil moisture (Lloyd and Taylor, 1994; Yan et al., 2016). High soil moisture might have contributed to the observed higher respiration rates, but cannot be seen as the sole explanatory factor. With a value of 2.5 % in 2021, substrate TOC remained close to its initial value of 1.5–2.5 %, possibly showing some substrate ageing (accumulation of organic matter from decomposing plants and animals), but then increased abruptly to 7.9 % in 2022 and remained elevated thereafter. Higher nocturnal respiration during 2022–2023 (1.27 times the median of the previous years) is consistent with the increase in substrate TOC. Other studies indicate that high-organic GR substrates show substantially greater CO_2 efflux than low-organic substrates (Halim et al., 2022). A mass-balance comparison underpins that atmospheric carbon sequestration, as estimated from NEE observation, which is cumulatively added to the initial substrate TOC, agrees well with measured substrate TOC until 2021 (Fig. 11b). Besides the substrate, carbon from atmospheric sequestration is stored in above- and belowground biomass. In Fig. 11b, we show that even if we allocate the entire annual NEE to the substrate and do not consider export of carbon via runoff, the abrupt rise of TOC after 2022 cannot be explained by atmospheric sequestration alone.

This suggests external carbon inputs - such as unremoved plant litter after maintenance by gardeners (1–2 times per year, cf. Heusinger and Weber, 2017b) or application of carbon-rich material (e.g. organic fertilisers) - as the most plausible cause, although no specific maintenance events were reported by the operator of the GR. Hence, we argue that the observed shift from a robust carbon sink to carbon-neutral conditions was primarily driven by the sudden increase in substrate TOC, which originated from sources other than atmospheric CO_2 sequestration. Assuming that the threshold at which the carbon sink function of the GR disappears (i.e. NEE ≈ 0 g C m^{-2}) is defined by the substrate TOC of 7.9 % in 2022, it would take at least 32 years to reach that value when extrapolating the time series from 2022 onwards at an average rate of sequestration of 121 g C m^{-2} a^{-1} (the average rate of sequestration for the years 2015–2021). Further assessment is not possible after 2023 due to the installation of photovoltaics and the resulting alteration of the GR system.

https://doi.org/10.5194/egusphere-2026-942
Preprint. Discussion started: 4 March 2026

4.2 Water exchange and energy partitioning

During the 9-year study period, we found that 49 % of the precipitation resulted in GR runoff, meaning that 51 % was retained. Except for the years 2018 and 2023, annual retention ranged between 49–58 %. The retention capacity of the BER GR is within the range of values found in other studies for extensive GRs: Schultz et al. (2018) studied runoff patterns from two extensive GRs with substrate depths of 7.5 and 12.5 cm in Portland, Oregon, USA, for a full annual cycle. From a total of 808 mm precipitation, 23.2 (7.5 cm GR) and 32.9 % (12.5 cm GR) was retained. In 2023, precipitation sum for BER (9 cm substrate depth) was similar (736 mm), and retention was 38 % of the annual precipitation sum. Stovin et al. (2012) reported a value of 50 % retention from a UK extensive GR test bed and VanWoert et al. (2005) 61 % on a roof platform with full vegetation coverage. Our data suggests that high annual precipitation sums lead to lower annual retention. Studies report that meteorological conditions, e.g. precipitation sum, and other factors such as GR design may have a considerable influence on the retention capacity of GRs (Liu et al., 2019; Stovin, 2010; Schultz et al., 2018). Our results suggest that the water storage of the GR provides sufficient capacity to enhance ET and reduce runoff, which in turn has the potential to reduce the burden on wastewater structures as well as the risk of flooding in urban areas.

Since substrate water availability not only determines the hydrological performance but also directly affects the energy and carbon fluxes of the system, the interaction between water content, Bowen ratio, and carbon assimilation was further examined. When β reaches values ≥ 2 during summer and ≥ 3 during spring, net carbon assimilation by the GR is reduced. This is the case when VWC is below a critical threshold of ≈ 0.05 m^3 m^{-3}. The three variables are coupled: Low VWC reduce ET, resulting in increased partitioning of available energy into sensible heat flux, i.e. higher β, as well as lower net carbon assimilation. With regard to the ecosystem services of extensive GR, it would therefore be advisable to keep VWC values above that threshold to preserve the cooling effect and to increase carbon assimilation by the GR. This could be achieved through a sustainable automated irrigation, e.g. using on-site harvested rainwater, which activates during dry conditions (e.g. Heusinger et al., 2018).

https://doi.org/10.5194/egusphere-2026-942
Preprint. Discussion started: 4 March 2026

5 Summary and conclusions

Over a 9-year period from 2015 to 2023, the exchange of carbon, water, and energy between an extensive green roof and the atmosphere was analysed using the eddy-covariance technique. The long-term data provide detailed insights into the coupled exchange dynamics of the green roof ecosystem. Over the study period, the site was a moderate carbon sink with an annual average uptake of -92 g C m^{-2}, and an annual range of -154 to +8 g C m^{-2}. The shift from net carbon uptake to a slight net release of carbon in the final two years of the study period is primarily due to higher respiration rates in 2022 and 2023. Our data suggests that the higher respiration rates are linked to an abrupt increase in the substrate organic carbon content, caused by external carbon input.

The GR retained 51 % of the precipitation over the study period, suggesting that extensive green roofs effectively reduce urban runoff volume and enhance evapotranspiration. The analysis proved that water, carbon, and energy fluxes in green roof ecosystems are tightly coupled: low substrate moisture contents limit evapotranspiration rates, increase sensible heat fluxes (higher Bowen ratio), and suppress carbon assimilation. A substrate water availability of approximately 0.05 m^3 m^{-3} is critical for maintaining evaporative cooling and (high) carbon assimilation during summer. From a practical perspective and with a view to climate adaptation and mitigation, maintaining the volumetric water content above this level - potentially through automated, rainwater-based irrigation - can optimise ecosystem services. These findings emphasise the multifaceted environmental benefits of green roofs while also pointing to structural constraints such as shallow substrate and (limited) water availability, especially in warm and dry periods.

The present study closes a knowledge gap by providing multi-year continuous datasets of carbon, water and energy fluxes from an extensive green roof, highlighting both its potential and limitations as a component of sustainable urban green infrastructure. The findings also demonstrate the importance of integrated flux monitoring for the evaluation of green roof performance. Future research could focus on quantifying the long-term evolution of substrate carbon and its implications for roof carbon budgets. Moreover, improving the attribution of flux variability to meteorological and substrate conditions remains an important research need.

https://doi.org/10.5194/egusphere-2026-942
Preprint. Discussion started: 4 March 2026

Appendix A

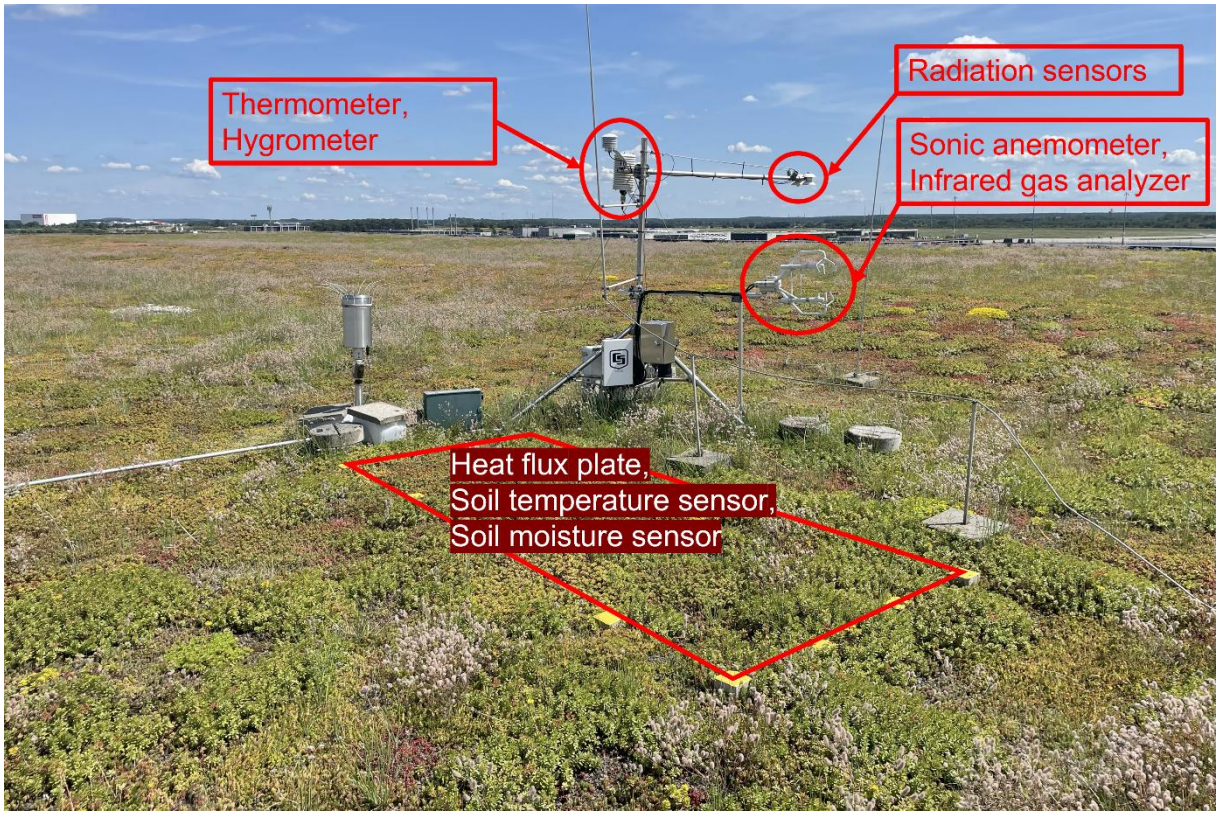

Figure A1. Photo of the green roof and measurement setup taken on 18.07.2024.

https://doi.org/10.5194/egusphere-2026-942
Preprint. Discussion started: 4 March 2026

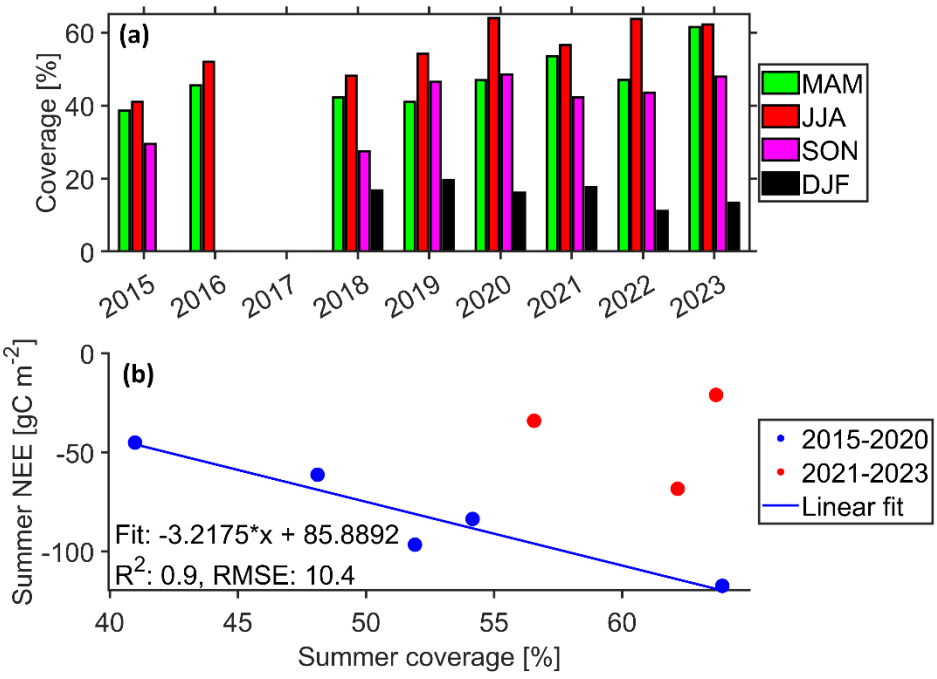

Figure A2. (a) Development of the green roof plant coverage over the years. Overall plant coverage was estimated from photographs taken at regular intervals (usually every 1–2 months) from up to 11 fixed spots distributed evenly throughout the GR. A mean value for a season was only calculated when there were at least two data points within a season, and on those days, at least 8 spots were captured. DJF = winter, MAM = spring, JJA = summer, SON = autumn. (b) Relationship between plant coverage and net ecosystem exchange (NEE) for summer. A linear fit is shown for the data 2015–2020.

https://doi.org/10.5194/egusphere-2026-942
Preprint. Discussion started: 4 March 2026

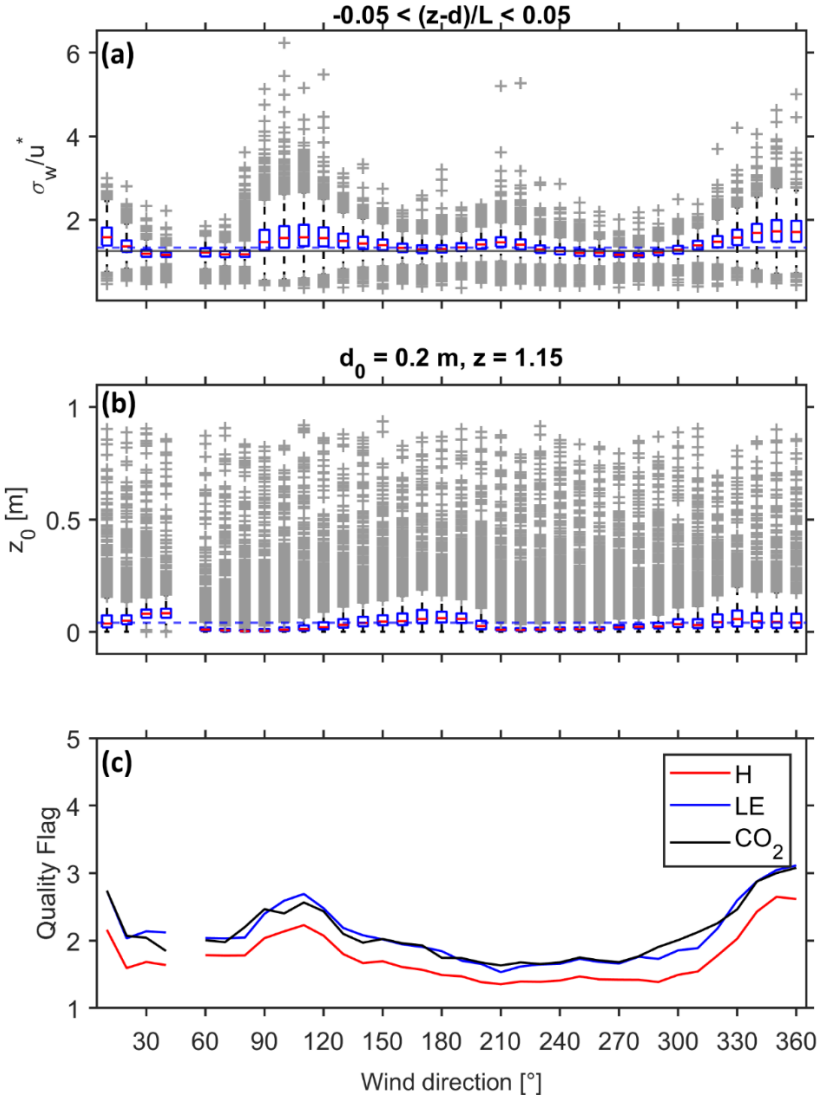

Figure A3. (a) Integral turbulence characteristic, given by the ratio of the standard deviation of the vertical wind velocity (σ_w) to friction velocity (u*) under neutral stratification. The grey line indicates a value of 1.25 proposed for well-developed homogeneous turbulence (Foken and Mauder, 2024), while the dashed, blue line shows the mean value from observations. (b) Roughness length (z_0) with mean value indicated by dashed, blue line. (c) Mean quality flag values, calculated according to Foken et al. (2005), of sensible- (H) and latent- (LE) heat flux as well as CO_2 flux for 10 ° wind direction classes after rejection of quality flags ≥ 7. Boxplots are given for 10° wind direction classes with the median (red line) as well as the interquartile range (box) and the range within which values are not considered outliers (vertical dashed lines). Outliers are depicted by a red "+".

https://doi.org/10.5194/egusphere-2026-942
Preprint. Discussion started: 4 March 2026

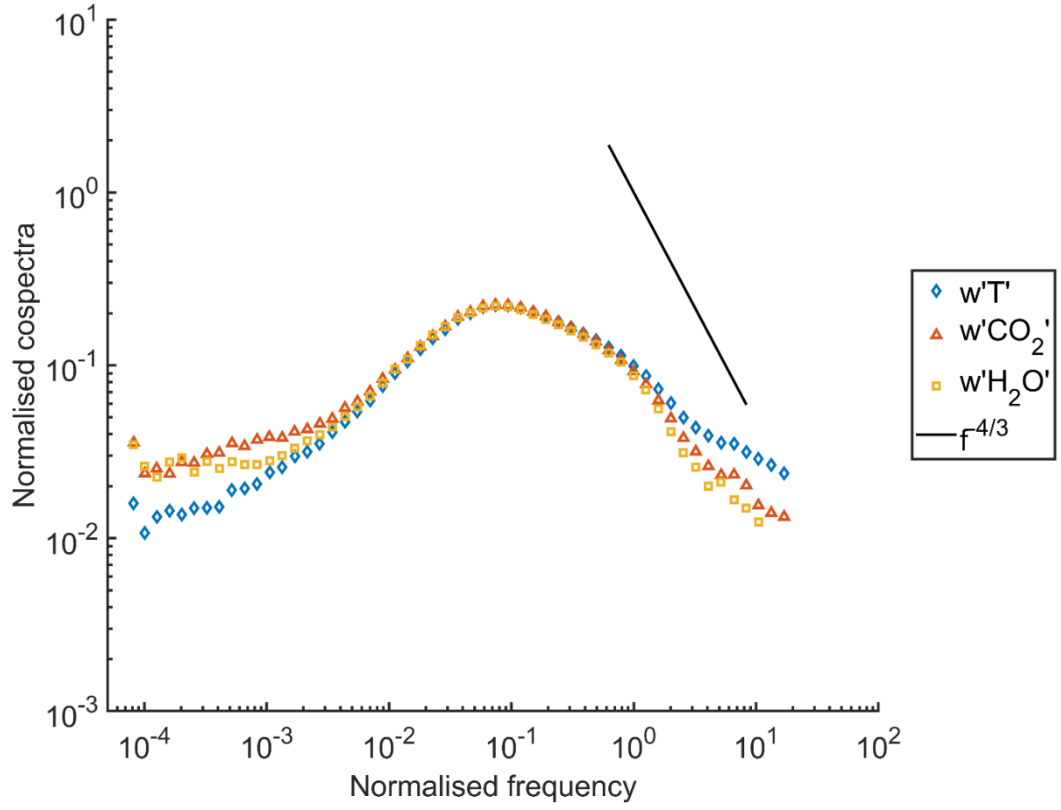

Figure A4. Cospectra (sensible heat, CO_2, H_2O) for unstable stratification (-650 m < L < 0 m) for the time period of 01.04.2022–31.03.2023.

450

https://doi.org/10.5194/egusphere-2026-942
Preprint. Discussion started: 4 March 2026

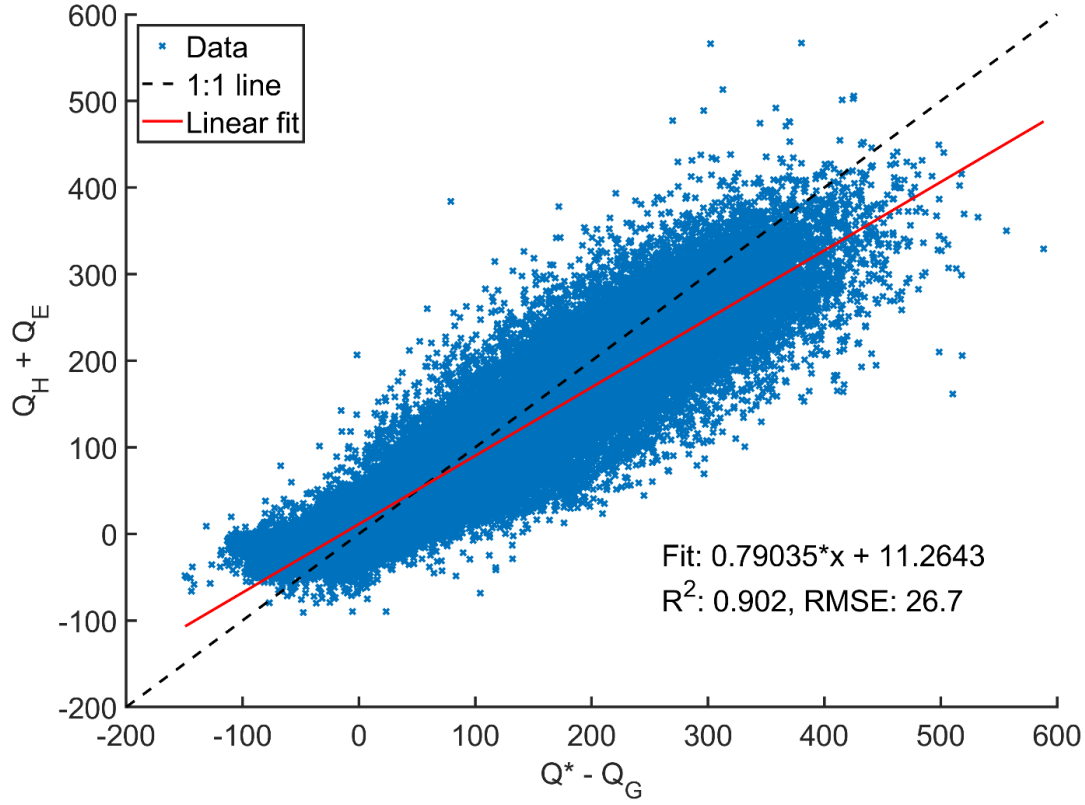

Figure A5. Half-hourly values of available energy ($Q^* - Q_G$) plotted against the sum of turbulent heat fluxes ($Q_H + Q_E$). A linear regression has been fit (red line) and the 1:1 line (dashed) plotted.

https://doi.org/10.5194/egusphere-2026-942
Preprint. Discussion started: 4 March 2026

Table A1: Results from the Spearman Rank Correlation test and the Mann-Kendall test.

	Spearman		Mann-Kendall	
	ρ	p-value	τ	p-value
Net assimilation rate	0.183	0.644	0.111	0.761
Net respiration rate	0.667	0.083	0.500	0.109
Sink season NEE	0.317	0.410	0.167	0.612
Source season NEE	0.786	0.028	0.643	0.031

https://doi.org/10.5194/egusphere-2026-942
Preprint. Discussion started: 4 March 2026

Data availability

Data will be made available on request

Author contributions

Niklas Markolf: Conceptualization, Investigation, Methodology, Validation, Data curation, Formal analysis, Software, Visualization, Writing (original draft preparation)

Stephan Weber: Conceptualization, , Methodology, Validation, Funding acquisition, Project administration, Resources, Supervision, Writing (review and editing)

Competing interests

The authors declare that they have no conflict of interest.

Financial support

This research was funded by the German Research Foundation (DFG) under contract 505703010 (GREENVELOPES).

https://doi.org/10.5194/egusphere-2026-942
Preprint. Discussion started: 4 March 2026

References

Akbari, H. and Rose, L. S.: Urban Surfaces and Heat Island Mitigation Potentials, JHES, 11, 85–101, https://doi.org/10.1618/jhes.11.85, 2008.

Aubinet, M., Vesala, T., and Papale, D. (Eds.): Eddy Covariance: A Practical Guide to Measurement and Data Analysis, Springer Netherlands, Dordrecht, 2012.

Birch, H. F.: The effect of soil drying on humus decomposition and nitrogen availability, Plant Soil, 10, 9–31, https://doi.org/10.1007/BF01343734, 1958.

Bruno, G., Avanzi, F., Gabellani, S., Ferraris, L., Cremonese, E., Galvagno, M., and Massari, C.: Disentangling the role of subsurface storage in the propagation of drought through the hydrological cycle, Advances in Water Resources, 169, 104305, https://doi.org/10.1016/j.advwatres.2022.104305, 2022.

Croux, C. and Dehon, C.: Influence functions of the Spearman and Kendall correlation measures, Stat Methods Appl, 19, 497–515, https://doi.org/10.1007/s10260-010-0142-z, 2010.

Falge, E., Baldocchi, D., Olson, R., Anthoni, P., Aubinet, M., Bernhofer, C., Burba, G., Ceulemans, R., Clement, R., Dolman, H., Granier, A., Gross, P., Grünwald, T., Hollinger, D., Jensen, N.-O., Katul, G., Keronen, P., Kowalski, A., Lai, C. T., Law, B. E., Meyers, T., Moncrieff, J., Moors, E., Munger, J., Pilegaard, K., Rannik, Ü., Rebmann, C., Suyker, A., Tenhunen, J., Tu, K., Verma, S., Vesala, T., Wilson, K., and Wofsy, S.: Gap filling strategies for defensible annual sums of net ecosystem exchange, Agricultural and Forest Meteorology, 107, 43–69, https://doi.org/10.1016/S0168-1923(00)00225-2, 2001a.

Falge, E., Baldocchi, D., Olson, R., Anthoni, P., Aubinet, M., Bernhofer, C., Burba, G., Ceulemans, R., Clement, R., Dolman, H., Granier, A., Gross, P., Grünwald, T., Hollinger, D., Jensen, N.-O., Katul, G., Keronen, P., Kowalski, A., Ta Lai, C., Law, B. E., Meyers, T., Moncrieff, J., Moors, E., William Munger, J., Pilegaard, K., Rannik, Ü., Rebmann, C., Suyker, A., Tenhunen, J., Tu, K., Verma, S., Vesala, T., Wilson, K., and Wofsy, S.: Gap filling strategies for long term energy flux data sets, Agricultural and Forest Meteorology, 107, 71–77, https://doi.org/10.1016/S0168-1923(00)00235-5, 2001b.

Ferreira, C. S. S., Potočki, K., Kapović-Solomun, M., and Kalantari, Z.: Nature-Based Solutions for Flood Mitigation and Resilience in Urban Areas, in: Nature-Based Solutions for Flood Mitigation, edited by: Ferreira, C. S. S., Kalantari, Z., Hartmann, T., and Pereira, P., Springer International Publishing, Cham, 59–78, https://doi.org/10.1007/698_2021_758, 2022.

Foken, T. and Mauder, M.: Grundgleichungen der atmosphärischen Turbulenz, in: Angewandte Meteorologie: Mikrometeorologische Methoden, Springer Berlin Heidelberg, Berlin, Heidelberg, 75, https://doi.org/10.1007/978-3-662-68333-0_2, 2024.

Foken, T., Göockede, M., Mauder, M., Mahrt, L., Amiro, B., and Munger, W.: Post-Field Data Quality Control, in: Handbook of Micrometeorology: A Guide for Surface Flux Measurement and Analysis, edited by: Lee, X., Massman, W., and Law, B., Springer Netherlands, Dordrecht, 181–208, https://doi.org/10.1007/1-4020-2265-4_9, 2005.

Formanek, S., Mauss, K., Peritsch, M., and Schultes, C.: Green Market Report: Bauwerksbegrünung in Österreich 2019-2022, Vienna, 2024.

Francis, L. F. M. and Jensen, M. B.: Benefits of green roofs: A systematic review of the evidence for three ecosystem services, Urban Forestry & Urban Greening, 28, 167–176, https://doi.org/10.1016/j.ufug.2017.10.015, 2017.

Fratini, G. and Mauder, M.: Towards a consistent eddy-covariance processing: an intercomparison of EddyPro and TK3, Atmos. Meas. Tech., 7, 2273–2281, https://doi.org/10.5194/amt-7-2273-2014, 2014.

Getter, K. L., Rowe, D. B., Robertson, G. P., Cregg, B. M., and Andresen, J. A.: Carbon sequestration potential of extensive green roofs, Environmental science & technology, 43, 7564–7570, https://doi.org/10.1021/es901539x, 2009.

Gilmanov, T. G., Soussana, J. F., Aires, L., Allard, V., Ammann, C., Balzarolo, M., Barcza, Z., Bernhofer, C., Campbell, C. L., Cernusca, A., Cescatti, A., Clifton-Brown, J., Dirks, B., Dore, S., Eugster, W., Fuhrer, J., Gimeno, C., Gruenwald, T., Haszpra, L., Hensen, A., Ibrom, A., Jacobs, A., Jones, M. B., Lanigan, G., Laurila, T., Lohila, A., Manca, G., Marcolla, B., Nagy, Z., Pilegaard, K., Pinter, K., Pio, C., Raschi, A., Rogiers, N., Sanz, M. J., Stefani, P., Sutton, M., Tuba, Z.,

https://doi.org/10.5194/egusphere-2026-942
Preprint. Discussion started: 4 March 2026

Valentini, R., Williams, M. L., and Wohlfahrt, G.: Partitioning European grassland net ecosystem CO2 exchange into gross primary productivity and ecosystem respiration using light response function analysis, Agriculture, Ecosystems & Environment, 121, 93–120, https://doi.org/10.1016/j.agee.2006.12.008, 2007.

Greve, P., Gudmundsson, L., Orlowsky, B., and Seneviratne, S. I.: A two-parameter Budyko function to represent conditions under which evapotranspiration exceeds precipitation, Hydrol. Earth Syst. Sci., 20, 2195–2205, https://doi.org/10.5194/hess-20-2195-2016, 2016.

Grossiord, C., Buckley, T. N., Cernusak, L. A., Novick, K. A., Poulter, B., Siegwolf, R. T. W., Sperry, J. S., and McDowell, N. G.: Plant responses to rising vapor pressure deficit, The New phytologist, 226, 1550–1566, https://doi.org/10.1111/nph.16485, 2020.

Halim, M. A., Vantellingen, J., Gorgolewski, A. S., Rose, W. K., Drake, J. A. P., Margolis, L., and Thomas, S. C.: Greenhouse gases and green roofs: carbon dioxide and methane fluxes in relation to substrate characteristics, Urban Ecosyst, 25, 487–498, https://doi.org/10.1007/s11252-021-01166-8, 2022.

Han, J., Yang, Y., Roderick, M. L., McVicar, T. R., Yang, D., Zhang, S., and Beck, H. E.: Assessing the Steady-State Assumption in Water Balance Calculation Across Global Catchments, Water Resources Research, 56, https://doi.org/10.1029/2020WR027392, 2020.

Hansen, P., Heusinger, J., and Weber, S.: Carbon and water exchange in extensive green roofs: A comparison between eddy covariance and soil flux chamber observations, Urban Forestry & Urban Greening, 113, 129099, https://doi.org/10.1016/j.ufug.2025.129099, 2025.

Heusinger, J. and Weber, S.: Surface energy balance of an extensive green roof as quantified by full year eddy-covariance measurements, The Science of the total environment, 577, 220–230, https://doi.org/10.1016/j.scitotenv.2016.10.168, 2017a.

Heusinger, J. and Weber, S.: Extensive green roof CO2 exchange and its seasonal variation quantified by eddy covariance measurements, The Science of the total environment, 607-608, 623–632, https://doi.org/10.1016/j.scitotenv.2017.07.052, 2017b.

Heusinger, J., Sailor, D. J., and Weber, S.: Modeling the reduction of urban excess heat by green roofs with respect to different irrigation scenarios, Building and Environment, 131, 174–183, https://doi.org/10.1016/j.buildenv.2018.01.003, 2018.

Kljun, N., Calanca, P., Rotach, M. W., and Schmid, H. P.: A simple two-dimensional parameterisation for Flux Footprint Prediction (FFP), Geosci. Model Dev., 8, 3695–3713, https://doi.org/10.5194/gmd-8-3695-2015, 2015.

Klosterhalfen, A., Fellert, D., Koebsch, F., Kreilein, H., Markwitz, C., Mund, M., Peksa, M., Tiedemann, F., Tunsch, E., and Knohl, A.: Analysis of a 23-years Long Eddy-covariance Fluxes Dataset from a Mixed Deciduous Forest in Germany, EGU General Assembly 2023, https://doi.org/10.5194/egusphere-egu23-13689, 2023.

Konopka, J., Heusinger, J., and Weber, S.: Extensive Urban Green Roof Shows Consistent Annual Net Uptake of Carbon as Documented by 5 Years of Eddy-Covariance Flux Measurements, J Geophys Res Biogeosci, 126, https://doi.org/10.1029/2020JG005879, 2021.

Kuronuma, T. and Watanabe, H.: Relevance of Carbon Sequestration to the Physiological and Morphological Traits of Several Green Roof Plants during the First Year after Construction, AJPS, 08, 14–27, https://doi.org/10.4236/ajps.2017.81002, 2017.

LI-COR Biosciences: Eddy Covariance Processing Software (EddyPro), 2022.

Liebethal, C., Huwe, B., and Foken, T.: Sensitivity analysis for two ground heat flux calculation approaches, Agricultural and Forest Meteorology, 132, 253–262, https://doi.org/10.1016/j.agrformet.2005.08.001, 2005.

Liu, W., Feng, Q., Chen, W., Wei, W., and Deo, R. C.: The influence of structural factors on stormwater runoff retention of extensive green roofs: new evidence from scale-based models and real experiments, Journal of Hydrology, 569, 230–238, https://doi.org/10.1016/j.jhydrol.2018.11.066, 2019.

Lloyd, J. and Taylor, J. A.: On the Temperature Dependence of Soil Respiration, Functional Ecology, 8, 315, https://doi.org/10.2307/2389824, 1994.

https://doi.org/10.5194/egusphere-2026-942
Preprint. Discussion started: 4 March 2026

Mann, G. and Landwehr, R.: BuGG-Marktreport Gebäudegrün 2024: Dach-, Fassaden- und Innenraumbegrünung Deutschland, 2024.

Markolf, N., Heusinger, J., and Weber, S.: Water storage levels and water storage capacity of an extensive green roof quantified from multi-year eddy covariance measurements, Ecological Engineering, 206, 107333, https://doi.org/10.1016/j.ecoleng.2024.107333, 2024.

McAdam, S. A. M. and Brodribb, T. J.: The evolution of mechanisms driving the stomatal response to vapor pressure deficit, Plant physiology, 167, 833–843, https://doi.org/10.1104/pp.114.252940, 2015.

Moncrieff, J. B., Massheder, J. M., Bruin, H. de, Elbers, J., Friborg, T., Heusinkveld, B., Kabat, P., Scott, S., Soegaard, H., and Verhoef, A.: A system to measure surface fluxes of momentum, sensible heat, water vapour and carbon dioxide, Journal of Hydrology, 188-189, 589–611, https://doi.org/10.1016/S0022-1694(96)03194-0, 1997.

Oke, T. R.: The energetic basis of the urban heat island, Quart J Royal Meteoro Soc, 108, 1–24, https://doi.org/10.1002/qj.49710845502, 1982.

Pereira, P., Yin, C., and Hua, T.: Nature-based solutions, ecosystem services, disservices, and impacts on well-being in urban environments, Current Opinion in Environmental Science & Health, 33, 100465, https://doi.org/10.1016/j.coesh.2023.100465, 2023.

Reichstein, M., Falge, E., Baldocchi, D., Papale, D., Aubinet, M., Berbigier, P., Bernhofer, C., Buchmann, N., Gilmanov, T., Granier, A., Grünwald, T., Havránková, K., Ilvesniemi, H., Janous, D., Knohl, A., Laurila, T., Lohila, A., Loustau, D., Matteucci, G., Meyers, T., Miglietta, F., Ourcival, J.-M., Pumpanen, J., Rambal, S., Rotenberg, E., Sanz, M., Tenhunen, J., Seufert, G., Vaccari, F., Vesala, T., Yakir, D., and Valentini, R.: On the separation of net ecosystem exchange into assimilation and ecosystem respiration: review and improved algorithm, Global Change Biology, 11, 1424–1439, https://doi.org/10.1111/j.1365-2486.2005.001002.x, 2005.

Schultz, I., Sailor, D. J., and Starry, O.: Effects of substrate depth and precipitation characteristics on stormwater retention by two green roofs in Portland OR, Journal of Hydrology: Regional Studies, 18, 110–118, https://doi.org/10.1016/j.ejrh.2018.06.008, 2018.

Soltanifard, H. and Amani-Beni, M.: The cooling effect of urban green spaces as nature-based solutions for mitigating urban heat: insights from a decade-long systematic review, Climate Risk Management, 49, 100731, https://doi.org/10.1016/j.crm.2025.100731, 2025.

Starry, O., Lea-Cox, J. D., Kim, J., and van Iersel, M. W.: Photosynthesis and water use by two Sedum species in green roof substrate, Environmental and Experimental Botany, 107, 105–112, https://doi.org/10.1016/j.envexpbot.2014.05.014, 2014.

Stovin, V.: The potential of green roofs to manage Urban Stormwater, Water and Environment Journal, 24, 192–199, https://doi.org/10.1111/j.1747-6593.2009.00174.x, 2010.

Stovin, V., Vesuviano, G., and Kasmin, H.: The hydrological performance of a green roof test bed under UK climatic conditions, Journal of Hydrology, 414-415, 148–161, https://doi.org/10.1016/j.jhydrol.2011.10.022, 2012.

Teemusk, A., Kull, A., Kanal, A., and Mander, Ü.: Environmental factors affecting greenhouse gas fluxes of green roofs in temperate zone, The Science of the total environment, 694, 133699, https://doi.org/10.1016/j.scitotenv.2019.133699, 2019.

United Nations, Department of Economic and Social Affairs, Population Division: World Urbanization Prospects: The 2018 Revision (ST/ESA/SER.A/420), New York, 2019.

Ürge-Vorsatz, D., Chatterjee, S., Cabeza, L. F., and Molnár, G.: Global and regional estimation and evaluation of suitable roof area for solar and green roof applications, Developments in the Built Environment, 21, 100607, https://doi.org/10.1016/j.dibe.2025.100607, 2025.

VanWoert, N. D., Rowe, D. B., Andresen, J. A., Rugh, C. L., Fernandez, R. T., and Xiao, L.: Green Roof Stormwater Retention, J of Env Quality, 34, 1036–1044, https://doi.org/10.2134/jeq2004.0364, 2005.

Weber, S.: Comparison of in-situ measured ground heat fluxes within a heteorogeneous urban ballast layer, Theor. Appl. Climatol., 83, 169–179, https://doi.org/10.1007/s00704-005-0137-0, 2006.

https://doi.org/10.5194/egusphere-2026-942
Preprint. Discussion started: 4 March 2026

Xue, B.-L., Wang, L., Li, X., Yang, K., Chen, D., and Sun, L.: Evaluation of evapotranspiration estimates for two river basins on the Tibetan Plateau by a water balance method, Journal of Hydrology, 492, 290–297, https://doi.org/10.1016/j.jhydrol.2013.04.005, 2013.

Yan, Z., Liu, C., Todd-Brown, K. E., Liu, Y., Bond-Lamberty, B., and Bailey, V. L.: Pore-scale investigation on the response of heterotrophic respiration to moisture conditions in heterogeneous soils, Biogeochemistry, 131, 121–134, https://doi.org/10.1007/s10533-016-0270-0, 2016.

Yang, S., Kong, F., Yin, H., Zhang, N., Tan, T., Middel, A., and Liu, H.: Carbon dioxide reduction from an intensive green roof through carbon flux observations and energy consumption simulations, Sustainable Cities and Society, 99, 104913, https://doi.org/10.1016/j.scs.2023.104913, 2023.